Journal of Materials Chemistry A

REVIEW

View Article Online
View Journal | View Issue

Cite this: *J. Mater. Chem. A*, 2018, **6**, 22411

TiO_2-based heterojunction photocatalysts for photocatalytic reduction of CO_2 into solar fuels

Longfu Wei,[a] Changlin Yu, *[bc] Qinghong Zhang,[a] Hong Liu[d] and Ye Wang *[a]

In the twenty-first century, global warming and energy shortage have become major global issues. Up to now, the utilization of CO_2 as a carbon source for the production of fuels and chemicals has received increased attention. The photocatalytic reduction of CO_2 into solar fuels has turned out to become one of the most promising and environmentally friendly methods. Well-defined heterojunction structures between two semiconductors with matching electronic band structures can effectively facilitate charge transfer and suppress the recombination of photogenerated electrons and holes, resulting in enhanced photocatalytic performance. This review focuses on the design and fabrication of TiO_2-based heterojunction photocatalysts and their recent progresses into developing solar fuels *via* the photocatalytic reduction of CO_2. The photocatalytic performances of a number of typical TiO_2-based heterojunction photocatalysts, *e.g.*, p–n, non-p–n, Z-scheme, TiO_2–metal, TiO_2–carbon, phase, facet, and other heterojunctions, are summarized and analyzed. The reaction mode and some typical photoreactors, *e.g.*, slurry photoreactor, optical-fiber photoreactor, monolith photoreactor, and optofluidic microreactor, are also presented and analyzed. In the end, we propose a perspective on the opportunities and challenges to design new types of photocatalysts and photoreactors for improving the photocatalytic reduction of CO_2.

Received 12th September 2018
Accepted 24th October 2018

DOI: 10.1039/c8ta08879a

rsc.li/materials-a

[a]*State Key Laboratory of Physical Chemistry of Solid Surfaces, College of Chemistry and Chemical Engineering, Xiamen University, 422 Siming South Road, Xiamen 361005, Fujian, China. E-mail: wangye@xmu.edu.cn*

[b]*Faculty of Environmental Science and Engineering, Guangdong University of Petrochemical Technology, Maoming 525000, Guangdong, China. E-mail: yuchanglinjx@163.com*

[c]*School of Metallurgy and Chemical Engineering, Jiangxi University of Science and Technology, 86 Hongqi Road, Ganzhou 341000, Jiangxi, China*

[d]*Key Laboratory for Water Quality and Conservation of the Pearl River Delta, Ministry of Education, Institute of Environmental Research at Greater Bay, Guangzhou University, Guangzhou 510000, Guangdong, China*

Longfu Wei received his MSc degree in chemical engineering in 2015 (with Professor Changlin Yu) from the Jiangxi University of Science and Technology. He is now pursuing his PhD degree under the supervision of Ye Wang at the State Key Laboratory of Physical Chemistry of Solid Surfaces, College of Chemistry and Chemical Engineering, Xiamen University. His main research interests lie in the fabrication of novel photocatalysts for CO_2 reduction.

Changlin Yu received his PhD degree in Industrial Catalysis from the Dalian Institute of Chemical Physics, Chinese Academy of Sciences, in 2007. He joined the Jiangxi University of Science and Technology, where he was promoted to a full professor in 2012. He was a visiting scholar at Carnegie Mellon University. His research interests are mainly focused on photocatalysis applications in environmental purification, water splitting, and CO_2 reduction, as well as nanomaterials for catalysis. He is author or co-author of more than 160 peer-reviewed papers with over 3000 citations with an H-index of ~32. He has been an Editor Member of the Chinese Journal of Catalysis since 2017.

1. Introduction

The recent fast-paced developments in the social economy and industrialization have given rise to the problems of environmental pollution and energy shortage. The emission of carbon dioxide (CO_2) is mainly caused by the combustion of fossil fuels, resulting in a continuous rise in the concentration of CO_2 in the atmosphere.[1–3] As a major greenhouse gas, CO_2 can cause global warming, leading to disastrous climatic conditions.[4] Hence, decreasing the emission of CO_2 and rationally utilizing CO_2 have become formidable and important research subjects around the world. It is well known that CO_2 is a very stable molecule with a nonpolar covalent bond.[5–11] The dissociation energy of C=O bond in the CO_2 molecule is ~750 kJ mol^{-1}, which is higher than C–H (~430 kJ mol^{-1}) and C–C (~336 kJ mol^{-1}) bonds.[12] CO_2 has high thermodynamic stability and kinetic inertness; further, it has very low solubility in water (~30 mM under room temperature and 1 atm).[13–15] Therefore, the activation and conversion of CO_2 pose a big challenge.

In the natural environment, green plants absorb solar energy and use CO_2 and H_2O as raw materials to manufacture carbohydrates with the simultaneous release of oxygen.[16–20] Inspired by this natural process, artificial photosynthesis has become a research hotspot, showing rapid developments. In the early stages of this research paradigm, Fujishima and Honda reported certain semiconductor photocatalysts dispersed in water for the photocatalytic reduction of CO_2.[21] In the past decade, many photocatalysts, *e.g.*, TiO_2,[22–26] g-C_3N_4,[27–31] $ZnIn_2S_4$,[32–35] Bi_2WO_6,[36–41] graphene (GR),[42–46] CdS,[47–50] $SrNb_2O_6$,[51] and ZnO,[52–54] have been investigated for the photocatalytic reduction of CO_2. Among these photocatalysts, TiO_2 is the most widely used due to its abundance, chemical stability, low cost, and resistance toward corrosion.[55,56] With a wide bandgap of ~3.2 eV, TiO_2 can only absorb UV light, which represents 3–5% of the entire sunlight spectrum; therefore, it significantly limits its utilization of solar light.[57] Many strategies have been used for improving its activity and extending its light absorption in the visible light region.[58–60] Wang *et al.* firstly reported that adding MgO or polyaniline onto Pt–TiO_2 could improve the production of CH_4 for the photocatalytic reduction of CO_2.[61–63] In another study, Wang *et al.* also reported the core–shell-structured Pt@Cu_2O/TiO_2 to produce CH_4 and CO for CO_2 reduction.[64]

The well-defined heterojunction between two semiconductors with matching electronic band structures can significantly enhance the separation of photogenerated electrons (e^-) and holes (h^+), thereby considerably enhancing the photocatalytic performance.[65–70]. Yu *et al.* first synthesized a novel Ag_2O/Ag_2CO_3-heterostructured photocatalyst *via* a one-step phase transformation method. The photocatalytic activity for decomposing methyl orange was 68 and 30 times higher than that of pure Ag_2CO_3 and Ag_2O, respectively.[71] Recent studies have found that the unique role of a heterojunction can effectively promote the activity during the photocatalytic reduction of CO_2 into solar fuels.[72–77]

In this review, we will focus on the fundamental principles involved in the photocatalytic reduction of CO_2 and highlight the recent advances in TiO_2-based heterojunction

Qinghong Zhang received her MSc degree in 1992 from the Nanjing University of China, and she obtained her PhD degree in 2002 from the Hiroshima University of Japan. She joined Xiamen University in 2002, and she was promoted to a full professor in 2010. Her research interests include the synthesis and characterization of novel catalytic materials.

Hong Liu received his PhD degree in Physical Chemistry from Zhejiang University in 1999. Following his post-doctoral experiences in the Dalian Institute of Chemical Physics, CAS, and Hong Kong Polytechnic University, he became an associate professor in Sun Yat-sen University and was promoted to a full professor in 2008. In 2011, he moved to the Chongqing Institute of Green and Intelligent Technology, CAS, and transferred to Guangzhou University in 2017. His research interests are mainly focused on (photo)electrochemical technologies and principles for wastewater treatment. He has published over 80 papers, written 2 books, and applied for over 10 patents.

Ye Wang received his PhD degree in 1996 from the Tokyo Institute of Technology. He worked at the Tokyo Institute of Technology, Tohoku University, and Hiroshima University during 1996–2000. He became a professor of Xiamen University in 2001. His research interests are mainly focused on catalysis for the efficient utilization of carbon resources (selective transformation of methane, syngas, biomass, and CO_2 into fuels and chemicals). He is the author or co-author of more than 165 peer-reviewed papers with over 11648 citations and an H-index of ~63. He has been the member of the International Catalysis Association Council and the associate editor of ACS Catalysis.

photocatalysts for the photocatalytic reduction of CO_2. Moreover, the reaction mode and some typical photoreactors, *e.g.*, slurry photoreactor, optical-fiber photoreactor, monolith photoreactor, and optofluidic microreactor, are further presented and analyzed. Future prospects on the opportunities, research directions, and remaining challenges for the photocatalytic reduction of CO_2 will be addressed in the last section. We believe this review can provide some useful guidelines for the further development of highly active heterojunction photocatalysts for the photocatalytic reduction of CO_2.

2. Fundamental understanding for photocatalytic reduction of CO_2

2.1 Thermodynamic analysis

Due to its very stable and low energy grade, the chemical transformation of CO_2 is highly unfavorable in thermodynamics.[78–80] The possible reactions that can occur in the photocatalytic reduction of CO_2 in an aqueous medium are listed in Table 1.[81,82] The enthalpy change (ΔH) of all the reactions are highly positive, indicating that the reactions are endothermic and it becomes difficult for the corresponding reactions to occur at ambient temperatures. The Gibbs free energy change (ΔG) is also highly positive and a spontaneous reaction cannot occur. Moreover, it is evident that the photocatalytic reduction of CO_2 can store more energy than splitting water. Therefore, the photocatalytic reduction of CO_2 into hydrocarbon fuels requires a powerful catalyst and a large energy input, which is a big challenge in CO_2 reduction.

Table 2 lists the thermodynamic potentials of different products for CO_2 reduction with the thermodynamic potentials *vs.* normal hydrogen electrode (NHE) at pH = 7 in an aqueous solution at 25 °C and 1 atm.[83–86] It clearly shows that the thermodynamic potential for the reduction of CO_2 to CO_2^- radicals is −1.9 V by one electron, indicating that the reaction is highly unfavorable. Owing to the structural differences between linear CO_2 and bent CO_2^- radicals, a large kinetic "overvoltage" for one electron reduction is required (in eqn (1)).[87] It is evident that the other reactions with multiple proton-coupled electron transfer steps have lower standard potentials than one electron reduction; therefore, the other reactions are more favorable.[88] Moreover, the thermodynamic potential of CO_2 to CH_4 is more thermodynamically feasible than that required to reduce H^+ to H_2. Therefore, the principle for the photocatalytic reduction of CO_2 toward fuels is relatively complex, and we assume that this process involves multiple proton-coupled electron transfers instead of a single electron transfer.[89] With the exception of the listed thermodynamic considerations, we also need to consider the kinetic challenges in the photocatalytic reduction of CO_2.[90] From the perspective of kinetics, H_2 formation from the reduction of H_2O is more favorable, which is a strong competing reaction when compared with CO_2 reduction. We often use selectivity (ratio of the number of electrons reacting with CO_2 reduction to the number of all the reaction electrons) to estimate the efficiency of CO_2 reduction. Therefore, the selectivity for CO_2 reduction is low.

Table 1 Possible reactions for the photocatalytic reduction of CO_2 [81,82]

Equation	Reaction	$\Delta H^\ominus$ (kJ mol^{-1})	$\Delta G^\ominus$ (kJ mol^{-1})
1	H_2O (l) → H_2 (g) + 1/2O_2 (g)	286	237
2	CO_2 (g) → CO (g) + 1/2O_2 (g)	283	257
3	CO_2 (g) + H_2O (l) → HCOOH (l) + 1/2O_2 (g)	270	286
4	CO_2 (g) + H_2O (l) → HCHO (l) + O_2 (g)	563	522
5	CO_2 (g) + 2H_2O (l) → CH_3OH (l) + 3/2O_2 (g)	727	703
6	CO_2 (g) + 2H_2O (l) → CH_4 (g) + 2O_2 (g)	890	818

Table 2 Thermodynamic potentials of CO_2 reduction into various products[83–86]

Equation	Reaction	E^0 (V) *vs.* NHE at pH = 7
1	$CO_2 + e^- \rightarrow CO_2^-$	−1.9
2	$CO_2 + 2H^+ + 2e^- \rightarrow CO + H_2O$	−0.53
3	$CO_2 + 4H^+ + 4e^- \rightarrow C + 2H_2O$	−0.20
4	$CO_2 + 2H^+ + 2e^- \rightarrow HCOOH$	−0.61
5	$CO_2 + 4H^+ + 4e^- \rightarrow HCHO + H_2O$	−0.48
6	$CO_2 + 6H^+ + 6e^- \rightarrow CH_3OH + H_2O$	−0.38
7	$CO_2 + 8H^+ + 8e^- \rightarrow CH_4 + 2H_2O$	−0.24
8	$2CO_2 + 9H^+ + 12e^- \rightarrow C_2H_5OH + 3H_2O$	−0.33
9	$2H^+ + 2e^- \rightarrow H_2$	−0.41

2.2 Reaction mechanism

It is well known that the energy band of a semiconductor is divided into conduction band (CB) and valence band (VB). In order to achieve the photocatalytic reduction of CO_2, a good photocatalyst should have suitable band positions and bandgap energy (E_g). Namely, the position of CB should be higher or more negative than the redox potential for CO_2 reduction, whereas the VB should be lower or more positive than the oxidation potential of H_2O to O_2,[91,92] and the absorbed light energy ($h\nu$) should be greater than or equal to E_g.[93,94] Fig. 1 shows the band positions of some typical semiconductors, such as TiO_2, Cu_2O, ZnO, CdS, and Bi_2WO_6.[95–101]

The typical processes for the photocatalytic reduction of CO_2 are described in Fig. 2.[101,102] The process involves the following three main steps. First, if $h\nu$ is greater than or equal to E_g under light irradiation, e^- and h^+ can be produced. Considering the visible light utilization in solar energy, we should develop visible light response photocatalysts that have narrow bandgap energies (E_g < 3.0 eV or λ > 415 nm).[103,104] Second, e^- and h^+ migrate toward the surface of the photocatalyst; at the same time, most e^- and h^+ may get consumed through the recombination in the surface and bulk. In order to obtain high overall efficiency, it is necessary to quickly transfer the e^-/h^+ pairs to the surface and suppress the recombination of e^-/h^+ pairs. Third, after migrating toward the surface of the photocatalyst,

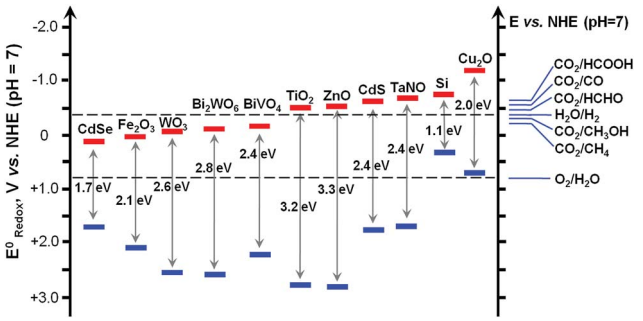

Fig. 1 Band positions of some semiconductors relative to the energy levels of CO_2 reduction. Reproduced from ref. 101 with permission from The Royal Society of Chemistry.

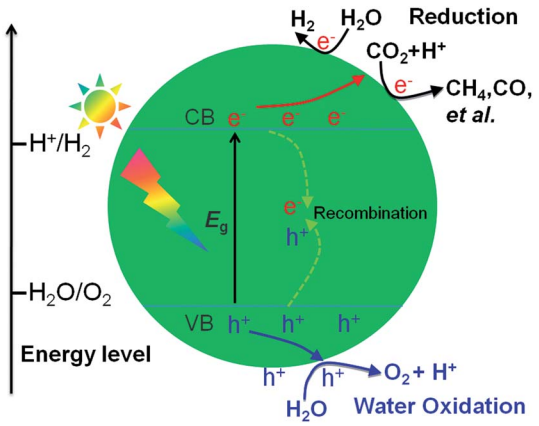

Fig. 2 Typical process of the photocatalytic reduction of CO_2. Reproduced from ref. 101 with permission from The Royal Society of Chemistry.

e^- and h^+ are used for the reduction and oxidation reactions, respectively. Here, e^- reacts with CO_2 and H^+ to produce CO and hydrocarbon fuels or only with H^+ to produce H_2. Further, h^+ reacts with H_2O to produce O_2, thereby accelerating H_2O oxidation and improving the separation of e^-/h^+ pairs to further enhance the activity. Increasing the activity of CO_2 reduction is a formidable challenge. The recombination of e^-/h^+ pairs is the determinant factor for photocatalytic activity.[105–109] Therefore, in order to obtain high activity for CO_2 reduction, we should formulate certain effective strategies, such as using a heterojunction to increase the charge transfer and restrain the recombination of e^-/h^+ pairs.[110–115]

3. Design and fabrication of a photoreactor

High photocatalytic activity is not only dependent on the catalyst but also on the photoreactor.[116] The reaction modes (solid–liquid and solid–vapor interfaces) and operation modes (batch, semi-batch, and continuous) are important parameters in the design and fabrication of a photoreactor. It is noteworthy that the operation parameters, *e.g.*, temperature, pressure, light source, and light intensity, play important roles in yielding high photocatalytic performances.

3.1 Reaction mode

The solid–liquid and solid–vapor interfaces are the two typical reaction modes for the photocatalytic reduction of CO_2. The schematic of two typical reaction modes are shown in Fig. 3. Fujishima and Honda conducted the pioneering work in the photocatalytic reduction of CO_2 at the solid–liquid interface,[21] and many researchers have since used this reaction mode.[117] The solid–liquid interface reaction mode is very simple, where the catalyst is dispersed in a solution. However, the solubility of CO_2 in water is very low, resulting in low photocatalytic activity. In order to overcome this issue, an alkaline medium has been used in a solution to increase the adsorption of CO_2. Nonetheless, CO_3^{2-} and HCO_3^- can be formed in an alkaline medium. Furthermore, CO_3^{2-} and HCO_3^- are difficult to reduce as compared to CO_2.[118] The solid–vapor interface reaction mode can circumvent these problems.[119] Wang *et al.* compared the solid–liquid interface and solid–vapor interface reaction mode of 0.5 wt% Pt–TiO_2 in the photocatalytic reduction of CO_2.[61,101] It was interesting to find that the CH_4 formation rate was 5.2 μmol g^{-1} h^{-1} in the solid–vapor interface, which was 3.7 times higher than that of the solid–liquid interface. However, the H_2 formation rate in the solid–vapor interface was lower than that of the solid–liquid interface. In the solid–vapor interface, the catalyst was exposed in a CO_2 atmosphere to avoid H_2 formation. Therefore, the selectivity for CO_2 reduction was much higher in the solid–vapor interface, which was more suitable for CO_2 reduction in the presence of H_2O.

3.2 A typical photoreactor

3.2.1 Slurry photoreactor. In Fig. 4a, a slurry photoreactor with a suspended catalyst is shown, which has been widely used in the photocatalytic reduction of CO_2.[120] It has some advantages, such as simple construction, high amount of catalyst, and low cost. Furthermore, it is possible to design and fabricate a large-capacity photoreactor. However, catalyst separation and circulation are drawbacks. Bai *et al.* first reported Mo-doped titanate nanotube (TNT) photocatalysts in a monoethanolamine solution with a slurry batch photoreactor under UVA (8 W, 63 mW cm^{-2}) irradiation for the photocatalytic reduction of CO_2 into CH_4 and CO.[121] It was clearly found that the molybdenum structure and oxygen vacancies played important roles in enhancing the photocatalytic performance. Maroto-Valer *et al.* fabricated 1 wt% Pd/0.01 wt% Rh–TiO_2 in a slurry batch annular reactor system under UVA irradiation.[122] The obtained quantum efficiency was about 0.002% and CH_4 formation rate was 0.03 μmol g^{-1} h^{-1}. In order to realize the separation of H_2 and O_2, Wu *et al.* designed a slurry reactor with two separate components for O_2 and H_2 evolution through a Nafion membrane (Fig. 4b).[123] Pt/$CuAlGaO_4$ or Pt/$SrTiO_3$:Rh served as the catalyst in CO_2 reduction to produce CO, and WO_3 was used as the oxidation catalyst for the oxidation of H_2O to produce O_2. This dual-photocatalyst system yielded high

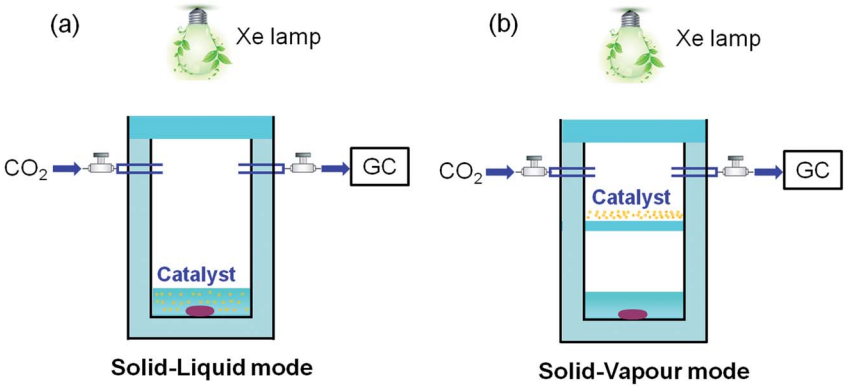

Fig. 3 Two typical reaction modes for the photocatalytic reduction of CO_2. (a) Solid–liquid interface reaction mode; (b) solid–vapor interface reaction mode. (a and b) Reproduced from ref. 61 with permission from the American Chemical Society and from ref. 101 with permission from The Royal Society of Chemistry.

quantum efficiency (0.0051%), which was 2.7 times higher than that of a single-photocatalyst system (0.0019%).

3.2.2 Optical-fiber photoreactor. A fixed-bed photoreactor can overcome the disadvantages of catalyst separation and circulation encountered in a slurry photoreactor. The catalysts are often coated onto the fixed supports, such as plates, beads, fibers, and the monolith.[5] The fibers can be used as a medium to uniformly deliver light onto the surface of the catalyst. In the optical-fiber photoreactor, the catalyst coated onto the fibers can direct light to enter along the fiber.[120] Fig. 5a shows the photograph of an optical-fiber photoreactor.[124] It has certain advantages such as high surface area and light utilization efficiency; however, it has a comparatively low surface area and low reactor volume with respect to the photocatalysis process. The $NiO/InTaO_4$ catalyst was prepared *via* the sol–gel method and then coated onto optical fibers and calcined to obtain a uniform layer.[124] The quantum efficiency of the optical-fiber reactor was 0.063%, which was much higher than that of the aqueous-phase reactor (0.0045%). In a similar work, Wu *et al.* also prepared Cu/TiO_2 for the photocatalytic reduction of CO_2 in an optical-fiber photoreactor, which showed the maximum CH_3OH formation rate (0.45 μmol g^{-1} h^{-1}) under 365 nm wavelength irradiation.[125] Wu *et al.* also reported metal-loaded TiO_2 films coated onto fibers in an optical-fiber photoreactor.[126] It was found that the maximum quantum efficiency was obtained with 1.2% Cu under 365 nm UV irradiation. In a further study, Wu *et al.* also researched the $Cu–Fe/TiO_2$ coated onto fibers; Fe and $Cu–TiO_2$ simultaneously promoted C_2H_4 formation and the quantum yield was about 0.024%.[127] A novel optical-fiber monolith reactor with multiple inverse lights for the photocatalytic reduction of CO_2 to produce CH_3OH was reported by Yang *et al.*[128] The maximum quantum efficiency was 0.0177%, which was higher than the internally illuminated monolith.

3.2.3 Monolith photoreactor. The monolith photoreactor has high surface area, low pressure drop, and ease in scale-up. The monolith is made up of many internal channels because of which it has a large surface area.[129] The catalyst is coated onto the walls of the channels. However, the light cannot efficiently penetrate through the channels because of the opacity of the honeycomb substrate; therefore, the length of the monolith reactor is limited. Fig. 5b shows the photograph of a monolith photoreactor.[130] Wu *et al.* reported that $NiO/InTaO_4$ was coated onto a precoated SiO_2 sublayer on the internal channels of the monolith for the photocatalytic reduction of CO_2 in a monolith photoreactor.[130] The maximum CH_3OH formation rate was 0.16 μmol g^{-1} h^{-1} under visible light irradiation. Moreover, the quantum efficiency of the monolith photoreactor was 0.012%, which was much higher than that of the optical-fiber reactor.

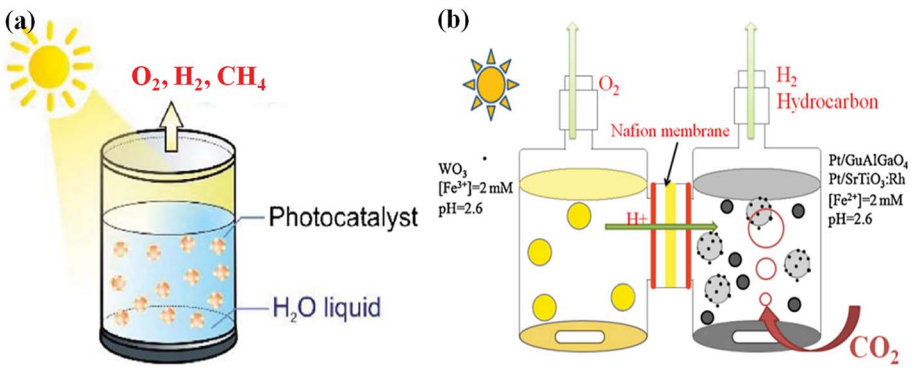

Fig. 4 Schematic diagram of (a) a typical slurry photoreactor and (b) a novel twin reactor system. (a) Reproduced from ref. 120 with permission from Elsevier. (b) Reproduced from ref. 123 with permission from Elsevier.

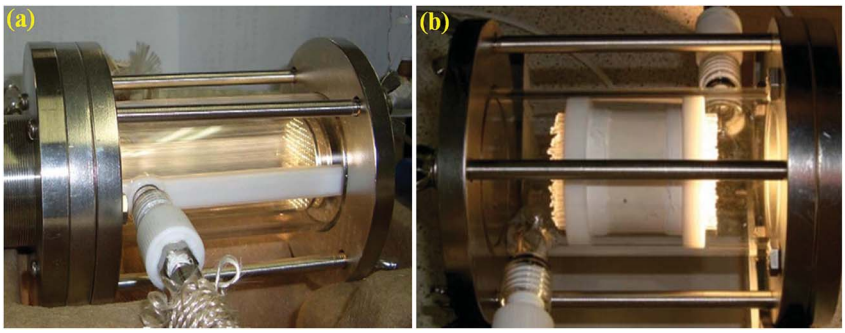

Fig. 5 Photographs of (a) an optical-fiber photoreactor and (b) a monolith photoreactor. (a) Reproduced from ref. 124 with permission from Elsevier. (b) Reproduced from ref. 130 with permission from The Royal Society of Chemistry.

Amin *et al.* reported montmorillonite (MMT)/TiO_2 for CO_2 reduction in a monolith photoreactor.[131] It exhibited a high CH_4 formation rate (139 μmol g^{-1} h^{-1}) when compared with a cell-type photoreactor (43 μmol g^{-1} h^{-1}) owing to the high illuminated surface area and light utilization. Tahir *et al.* developed a Cu- and N-doped TiO_2 nanocatalyst coated onto honeycomb monoliths for CO_2 reduction in a monolith photoreactor.[132] It was noteworthy that Cu and N could increase the activity and selectivity for CO_2 reduction to yield CO.

3.2.4 Optofluidic microreactor. An optofluidic microreactor has a precise control of flow, large surface area, enhanced mass transfer, and uniform light distribution; however, there exists a severe problem of limited throughput for practical applications. Fig. 6a and b show the schematic and photograph of an optofluidic planar microreactor, respectively.[133] Zhu *et al.* used an optofluidic planar microreactor to enhance the photocatalytic activity of a TiO_2 film in an alkaline environment.[133] The increase in the light intensity and NaOH concentration could increase the CH_3OH yields, and the increase in the liquid flow and catalyst loading initially improved and then decreased for the CH_3OH yields. In a similar study, Cheng *et al.* reported Cu–TiO_2 nanorods for the photocatalytic reduction of CO_2 in an optofluidic planar microreactor.[134] It had the maximum CH_3OH and CH_3CH_2OH yields with a flow rate of 2 mL min^{-1}. Fig. 6c and d show the schematic and photograph of an optofluidic membrane microreactor.[135] An optofluid with the membrane reactor technology for CO_2 reduction of TiO_2/carbon paper was reported by Chen *et al.*[135] The CH_3OH yield was much higher than those obtained from other types of photoreactors.

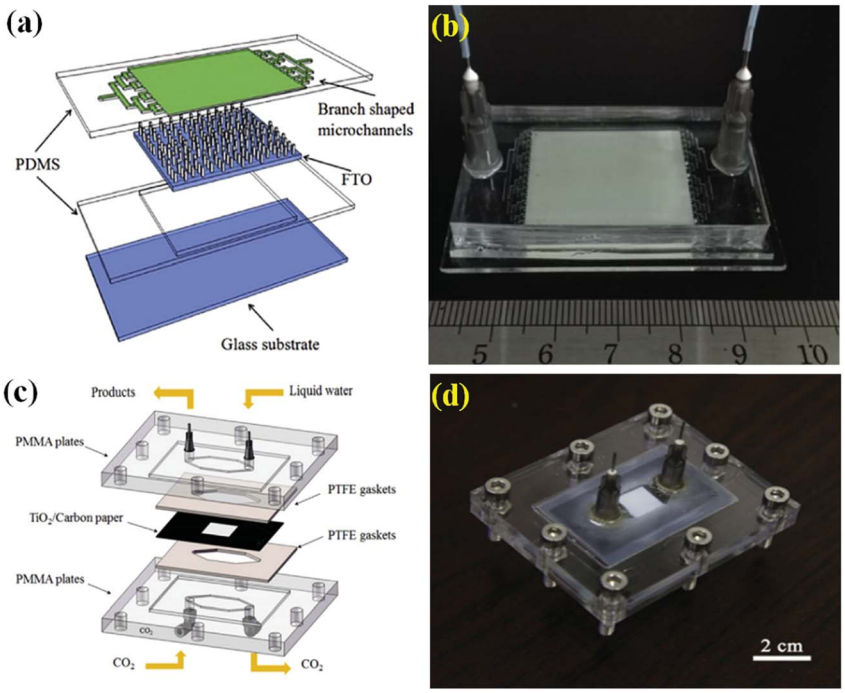

Fig. 6 Designs and photographs of (a and b) an optofluidic planar microreactor and (c and d) an optofluidic membrane microreactor. (a and b) Reproduced from ref. 134 with permission from Elsevier. (c and d) Reproduced from ref. 135 with permission from Elsevier.

4. Design and fabrication of TiO_2-based heterojunction photocatalysts

4.1 Coupling with other semiconductors

With regard to bare semiconductor photocatalysts, many strategies have been used to enhance their photocatalytic performance. A well-defined heterojunction structure between two semiconductors can accelerate the charge separation and suppress the recombination of e^-/h^+ pairs. A p–n heterojunction can be formed when n-type TiO_2 couples with some appropriate p-type semiconductor with matching electronic band structures. Fig. 7a shows the schematic diagram of the energy band structure and e^-/h^+ pair separation of a p–n heterojunction.[136] When n-type TiO_2 contacts with a p-type semiconductor, the diffusion of e^- and h^+ can form a space charge region at the interface. The difference in the electric potential can create a strong electric field to accelerate the charge separation of e^-/h^+ pairs. Except for p–n heterojunctions, other non-p–n heterojunctions exist. The schematic diagram of the energy band structure and e^-/h^+ pair separation of the non-p–n heterojunction are shown in Fig. 7b. Semiconductor A (SA) and semiconductor B (SB) are tightly bonded to form a heterojunction. Owing to the staggered alignment of the energy levels, e^- can transfer from the CB of SA to the CB of SB, whereas h^+ transfers from the VB of SB to the VB of SA under light irradiation. The non-p–n heterojunction is also suitable for the photocatalytic reduction of CO_2 into solar fuels, and TiO_2 is often used to fabricate such heterojunctions.

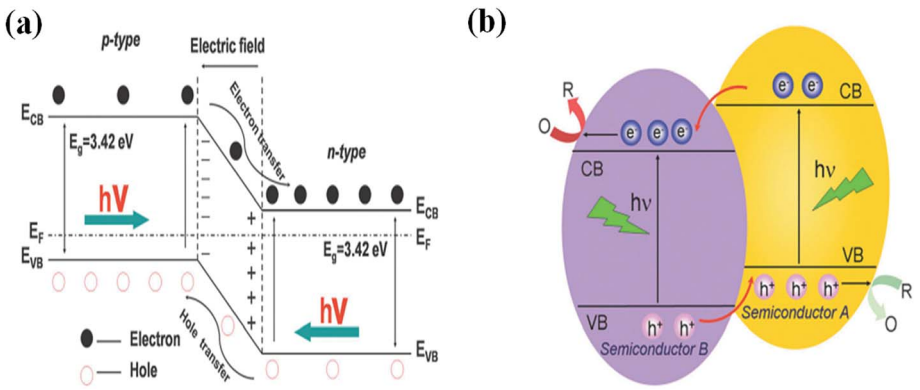

Fig. 7 Schematic diagram showing the energy band structure and e^-/h^+ pair separation in p–n (a) and non-p–n (b) heterojunctions. Reproduced from ref. 136 with permission from The Royal Society of Chemistry.

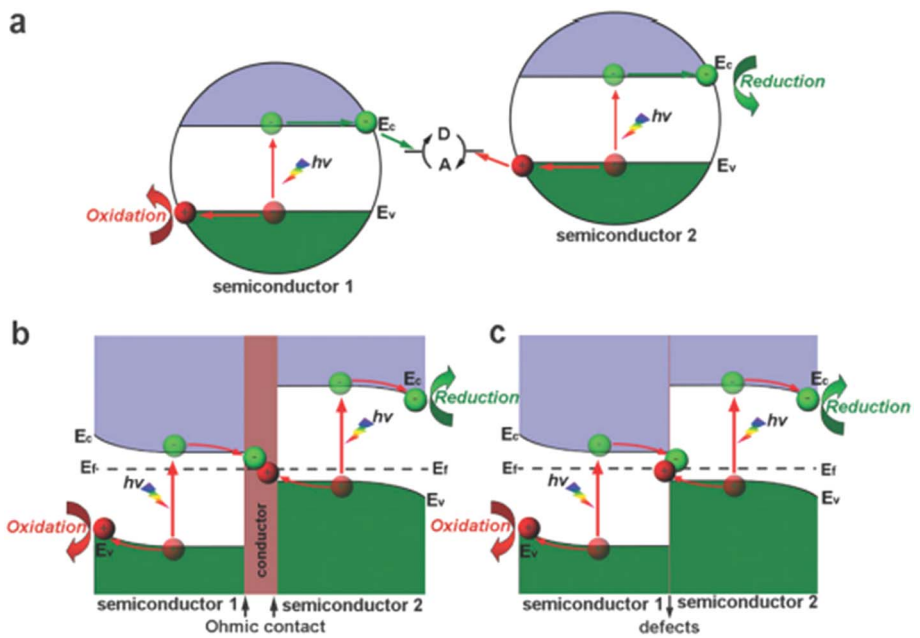

Fig. 8 Schematics of the (a) indirect Z-scheme structure mediated by redox pairs; (b) semiconductor–conductor–semiconductor all-solid-state Z-scheme structure; (c) semiconductor–semiconductor all-solid-state Z-scheme structure. Reproduced from ref. 138 with permission from The Royal Society of Chemistry.

Recently, another Z-scheme heterojunction system has aroused considerable interest.[137] It is typically made up of two semiconductors with staggered alignment of band structures. However, the CB and VB of the two semiconductors are only able to initiate reduction or oxidation of half of the reaction and unable to individually sustain the overall reactions. Fig. 8a shows the indirect Z-scheme heterojunction structure; e^- in the CB of semiconductor 1 recombines with h^+ in the VB of semiconductor 2; e^- in the CB of semiconductor 2 and h^+ in the VB of semiconductor 1 are utilized for the reduction and oxidation reactions, respectively.[138,139] Nevertheless, this structure can decrease the amount of e^- and h^+ available for the reactions and lead to low photocatalytic activity. The all-solid-state Z-scheme heterojunction structure can circumvent these problems. Fig. 8b and c show that a conductor serves as the electron mediator and many defects exist at the solid–solid interface. Recently, a novel double $Zn_3(VO_4)_2/Zn_2V_2O_7$/ZnO Z-scheme ternary vanadate heterojunction has been synthesized by Yu *et al.*, which exhibited high photocatalytic activity due to fast interfacial charge transfer and wider light response.[140] Table 3 summarizes and compares the typical TiO_2–semiconductor heterojunction photocatalysts for the photocatalytic reduction of CO_2.

4.1.1 p–n heterojunction. When TiO_2 and some p-type semiconductor are in contact, a strong electric field can be created. The produced electric field can accelerate charge separation and suppress the recombination of e^-/h^+ pairs. It is well known that copper compounds are very promising materials for the photocatalytic reduction of CO_2, and they are usually used to fabricate such p–n heterojunctions.

Table 3 Comparison of typical TiO_2–semiconductor heterojunction systems

Photocatalyst	Solvent	Light source	Time[a]	Formation rate[b]	QE[c] (%)	Reference
p–n heterojunction						
Cu_2O/TiO_2 porous	H_2O	Xe lamp ($\lambda > 300$ nm)	10	CH_4: 0.0284	—	145
Cu_2O/TiO_2 hollow nanospheres	H_2O	Xe lamp ($\lambda \geq 420$ nm)	8	CH_4: 0.16	—	146
Cu_2O/TiO_2	H_2O	UVA	1.5	CH_4: 0.024	—	147
$TiO_2/Ti_4O_9/Cu_2O$	H_2O	AM 1.5	5	CH_3OH: 0.586	—	148
Cu_2O/TiO_2 nanotube	H_2O	Xe Hg	6	CH_3OH: 9.19 μM mL^{-1} h^{-1}	1.731[d]	149
Cu_2O/TiO_2 nanotube	H_2O	Xe lamp ($\lambda < 420$ nm)	4	CH_4: 2 ppm h^{-1}	—	150
CuO/TiO_2 nanotube	H_2O	Hg lamp	3	CH_4 + CH_3OH	—	154
CuO/TiO_2	CH_3OH	Hg lamp (365 nm)	6	$HCOOCH_3$: 1600	—	157
CuO/TiO_2	1 M $KHCO_3$	UV lamps	6	CH_3OH: 442.5	19.23	158
CuO/TiO_2 hollow microspheres	H_2O	Hg UV lamp	24	CO: 5.47; CH_4: 0.36	CO: 1.285; CH_4: 0.747	159
Hybrid Cu_xO–TiO_2 ($x = 1, 2$)	H_2O	AM 1.5	1	CH_4: 0.22163	—	160
$CuO–TiO_{2-x}N_x$	H_2O	AM 1.5	3	CH_4: 41.3 ppm g^{-1} h^{-1}	—	161
GaP/TiO_2	H_2O	Xe lamp	24	CH_4: 2.46	—	163
Non p–n heterojunction						
CdS–TiO_2	Cyclohexanol	Xe lamp	10	Cyclohexyl formate: 20.2	—	169
CdS–TiO_2	2 M $NaNO_2$	Hg lamp	8	CO: 2; CH_4: 0375	—	171
CdS–TiO_2	2 M $NaNO_2$	Hg lamp (UV-visible)	8	CO: 1.3; CH_4: 0.1975	—	171
CdS–TiO_2 nanotube	2 M $NaNO_2$	Hg lamp (visible)	5	CH_3OH: 31.9	—	172
Bi_2S_3–TiO_2 nanotube	2 M $NaNO_2$	Xe lamp	5	CH_3OH: 44.9	—	172
PbS QDs–TiO_2	H_2O	Xe lamp	8	CH_4: 0.58; CO: 0.82; C_2H_6: 0.31	—	173
CeO_2–TiO_2	H_2O	Xe lamp	6	CO: 3.09	—	174
CeO_2–TiO_2	H_2O	Xe lamp	6	CH_4: 2200; CO: 13 600	—	175
TiO_2/ZnO	H_2O	Xe lamp	5	CH_4: 55	—	177
V and W doped TiO_2	H_2O	Xe lamp	4	CH_4: 0.22; CO: 1.91	0.063	178
$FeTiO_3/TiO_2$	2 M $NaNO_2$	Xe lamp ($\lambda > 300$ nm)	3	CH_3OH: 0.462	—	179
$FeTiO_3/TiO_2$	2 M $NaNO_2$	Xe lamp ($\lambda > 400$ nm)	3	CH_3OH: 0.432	—	179
Au_3Cu@$SrTiO_3/TiO_2$	$N_2H_4 \cdot H_2O$	Xe lamp	6	CO: 3770; CH_4: 421.2	2.51	180
TiO_2/g-C_3N_4	H_2O	Hg lamp	8	CH_4: 8.8; CO: 2.9	—	181
g-C_3N_4–N-TiO_2	H_2O	Xe lamp	12	CO: 12.28	—	182
$AgBr/TiO_2$	0.2 M $KHCO_3$	Xe lamp	5	CH_4: 128.56; CH_3OH: 77.87; CH_3CH_2OH: 13.28; CO: 32.14	—	183
Z-scheme heterojunction						
Si/TiO_2	H_2O	Xe lamp	3	CH_3OH	18.1[d]	186
$ZnFe_2O_4/TiO_2$	Cyclohexanol	Hg lamp	8	Cyclohexyl formate: 22.26	—	187
CdS/rGO/TiO_2	H_2O	Xe lamp	10	CH_4: 0.12	—	188

[a] Irradiation time, h. [b] Formation rate, μmol g^{-1} h^{-1}. [c] Quantum efficiency (%). [d] Photonic efficiency (%).

Furthermore, copper compounds can improve the selectivity for CO_2 reduction.[141]

Cuprous oxide (Cu_2O) is a p-type semiconductor with a narrow direct bandgap (~2.0 eV), which is a promising material for CO_2 reduction.[142–144] Ye *et al.* synthesized a porous-structured Cu_2O/TiO_2 heterojunction *via* a two-step process as follows.[145] First, titanium tetrachloride ($TiCl_4$) was used as the Ti precursor and heated with microwave assistance at 200 °C for 40 min; then, porous TiO_2 was synthesized and dispersed into ethanol. Second, copper(II) acetylacetonate ($Cu(acac)_2$) was used as the Cu precursor and added into TiO_2 dispersions and treated with a microwave-solvothermal process at 200 °C for 40 min. Then, a porous Cu_2O/TiO_2 heterojunction was obtained. The BET surface area of Cu_2O/TiO_2 (206.3 $m^2\ g^{-1}$) was 4.04 and 1.04 times higher than that of P25 (51.1 $m^2\ g^{-1}$) and porous TiO_2 (198.2 $m^2\ g^{-1}$), respectively. Moreover, the amounts of adsorbed CO_2 of Cu_2O/TiO_2 (0.27 mL g^{-1}) was much higher than that of P25 (0.05 mL g^{-1}) and porous TiO_2 (0.12 mL g^{-1}). The photocatalytic performance was evaluated by the photocatalytic reduction of CO_2 under UV-vis light irradiation ($\lambda > 300$ nm). It was found that the highest CH_4 formation rate could be achieved by the Cu_2O/TiO_2 heterojunction catalyst. Fig. 9 shows the schematic of the charge transfer in the Cu_2O/TiO_2 heterojunction. The bandgaps of TiO_2 and Cu_2O were 3.2 and 2.1 eV, respectively. Under light irradiation, e^- could transfer from the CB of Cu_2O to the CB of TiO_2, whereas h^+ could transfer from the VB of TiO_2 to the VB of Cu_2O, resulting in promoted separation efficiency of the photogenerated e^- and h^+. This superior performance was attributed to the heterojunction with high separation efficiency of e^-/h^+ pairs, as well as high CO_2 adsorption and more active reaction sites in the porous structure.

Morphology is expected to play a unique role in the photocatalytic performance. In a previous study, He *et al.* first fabricated Cu_2O hollow nanospheres by a soft-template method and then loaded them onto TiO_2 through the *in situ* hydrolysis of $Ti(OBu)_4$ under ultrasonic conditions.[146] Fig. 10 shows the SEM and TEM images of Cu_2O and Cu_2O/TiO_2 heterojunction. The diameter of Cu_2O hollow nanospheres was about 80–120 nm, and the Cu_2O/TiO_2 heterojunction also retained the same hollow spheres and diameter. In this case, the highest CH_4 formation rate was obtained by the Cu_2O/TiO_2 heterojunction under visible light irradiation. Cu_2O in contact with TiO_2 could form a p–n heterojunction to yield the efficient separation of photoinduced charge carriers as well as stability. In another study, Wu *et al.* reported Cu dispersion over Cu_2O/TiO_2 for the photocatalytic reduction of CO_2 using a stirred batch annular reactor under UVA irradiation.[147] A volcano tendency was evident in the CH_4 yield loading with moderate Cu amounts. It was found that the largest CH_4 yield could be obtained with Cu loading amount of 0.03%. Recently, a novel example of multi-component pillared structures of Cu_2O-decorated TiO_2-pillared tetratitanate was synthesized by Nogueira *et al.*[148] The BET surface area of $TiO_2/Ti_4O_9/Cu_2O$ (171 $m^2\ g^{-1}$) was 6.84 and 1.18 times higher than that of $K_2Ti_4O_9$ (25 $m^2\ g^{-1}$) and TiO_2/Ti_4O_9 (145 $m^2\ g^{-1}$), respectively. $TiO_2/Ti_4O_9/Cu_2O$ exhibited the maximum CH_3OH formation rate, which was attributed to the synergistic effect induced by the pillaring $K_2Ti_4O_9$ with TiO_2 pillars and the loading of the Cu_2O cocatalyst; this yielded the heterojunction structure. These three components could generate e^- and h^+ under light irradiation. However, Cu_2O was the main photocatalyst to generate e^- and h^+ owing to its narrowest bandgap. Further, e^- in the CB of TiO_2 could transfer to the CB of $H_2Ti_4O_9$, which then coupled with h^+ in the VB of Cu_2O. Furthermore, e^- in the CB of Cu_2O reacted with the surface-adsorbed CO_2 and H^+ to produce CH_3OH and h^+ in the VB of TiO_2 reacted with H_2O to produce O_2 and H^+. The electric field at the heterojunction interfaces could accelerate the transfer of e^-/h^+ pairs and the onset of the absorption band of the semiconductor exhibited a red-shift to improve the CH_3OH formation rate.

Ji *et al.* used the electrodeposition method to deposit Cu_2O nanoparticles (NPs) onto TiO_2 nanotubes (NTs) to fabricate the

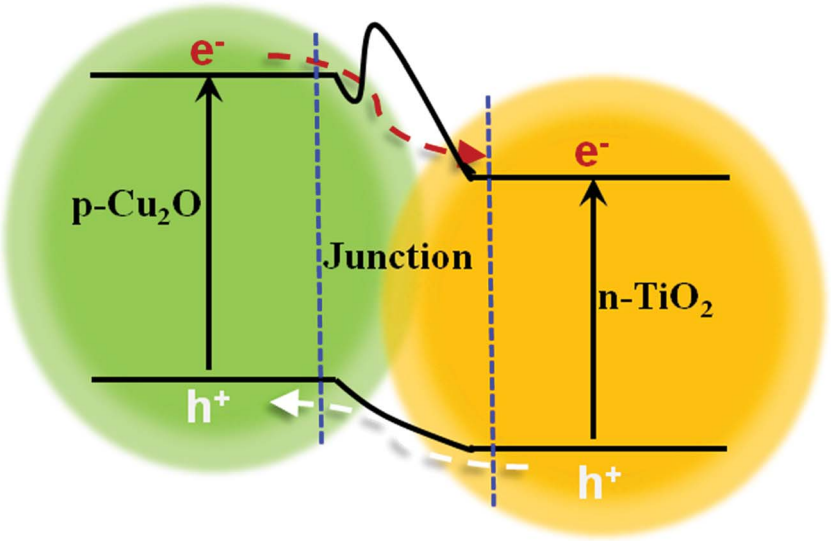

Fig. 9 Schematic of the charge transfer process of Cu_2O/TiO_2 heterojunction.

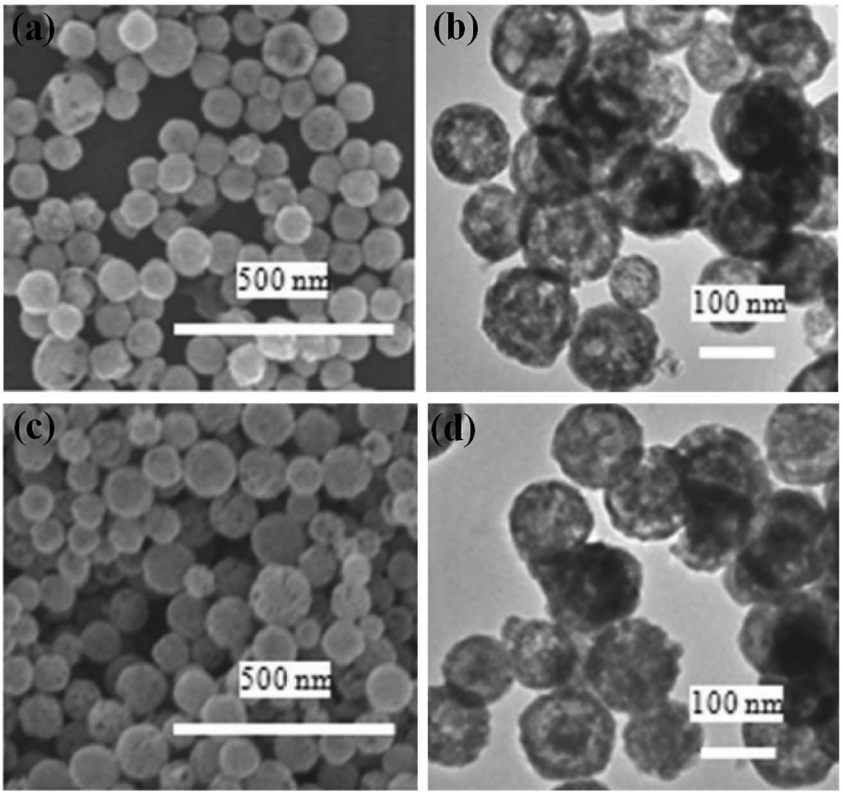

Fig. 10 SEM and TEM images of (a and b) Cu_2O and (c and d) Cu_2O/TiO_2 heterojunctions. Reproduced from ref. 146 with permission from Wiley-VCH.

Cu_2O/TiO_2 NT heterostructure.[149] Fig. 11a and b show the SEM images of the TiO_2 NTs. The average inner diameter and length of TiO_2 NTs were about 80 nm and 800 nm, respectively. Fig. 11c and d show the top and cross-sectional views of the Cu_2O/TiO_2 NT heterostructure. Cu_2O NPs with a polyhedral shape were formed on the surface of the TiO_2 NTs. Moreover, the Cu_2O NPs were wrapped around the inner and outer walls of the TiO_2 NTs. The Cu_2O/TiO_2 NTs exhibited stronger adsorption in the UV and visible light regions than that of TiO_2 NTs. The Cu_2O/TiO_2 NTs exhibited good photocatalytic activity for the photocatalytic reduction of CO_2 to CH_3OH, whereas the TiO_2 NTs were nearly inactive. The band energy values and charge carrier transfers of Cu_2O/TiO_2 NTs under visible light and UV-vis light irradiation are shown in Fig. 11e and f, respectively. It is well known that TiO_2 is a UV response semiconductor; therefore, only e^- can be generated in the CB of Cu_2O under visible light irradiation, which then transfers to the CB of TiO_2. However, both Cu_2O and TiO_2 can generate e^- under UV-vis light irradiation. Further, e^- in the CB of Cu_2O can transfer to the CB of TiO_2, whereas h^+ in the VB of TiO_2 can transfer to the VB of Cu_2O; thereafter, e^- and h^+ are effectively separated and the charge recombination process is suppressed. Due to the presence of Cu_2O/TiO_2 NT heterostructures, the photocatalytic activity was improved. In another report, Yu *et al.* fabricated the octahedral Cu_2O NPs deposited onto TiO_2 NTs by an electrochemical deposition method.[150] The largest CH_4 production rate was 2 ppm h^{-1} under visible light irradiation with the deposition time for 30 min. The TiO_2 NTs structure might offer high surface area and additional active sites. Furthermore, the Cu_2O NPs increased light absorption and enhanced the selectivity for CO_2 reduction into hydrocarbon products.

Cupric oxide (CuO) is a p-type semiconductor with a narrow direct bandgap, which is also a promising material for CO_2 reduction.[151–153] Previous studies have clarified that CuO is a good semiconductor to form a heterojunction due to its ability to be used as an electron trap. When CuO couples with TiO_2, an electric field is created at the interface. Therefore, the charge separation of e^- and h^+ is improved. Razali *et al.* reported CuO loaded onto TiO_2 NTs by a facile hydrothermal method.[154] The diameter and length of TiO_2 NTs with a fibrous-like structure were about 10 nm and several hundreds of nanometers, respectively. However, when CuO was loaded onto the TiO_2 NT, the morphology exhibited a considerable change, where they were tied together at the tip and exhibited a bundled, cobweb-like appearance. In the photocatalytic reduction of CO_2, the CuO/TiO_2 NT exhibited the highest CO_2 conversion (~100% for 2.5 h), which was higher than other metal oxide composites, such as ZnS/ZnO (45%) and immobilized MPc/ZnO (23%).[155,156] The CuO/TiO_2 NT heterojunction could improve the effective separation of e^-/h^+ pairs, resulting in improved activity. In another study, Xin *et al.* reported the $CuO–TiO_2$ photocatalyst for the photocatalytic reduction of CO_2 into $HCOOCH_3$ in the presence of CH_3OH, whereas CH_3OH was used as a sacrificial reagent to react with h^+.[157] The interfacial structure between

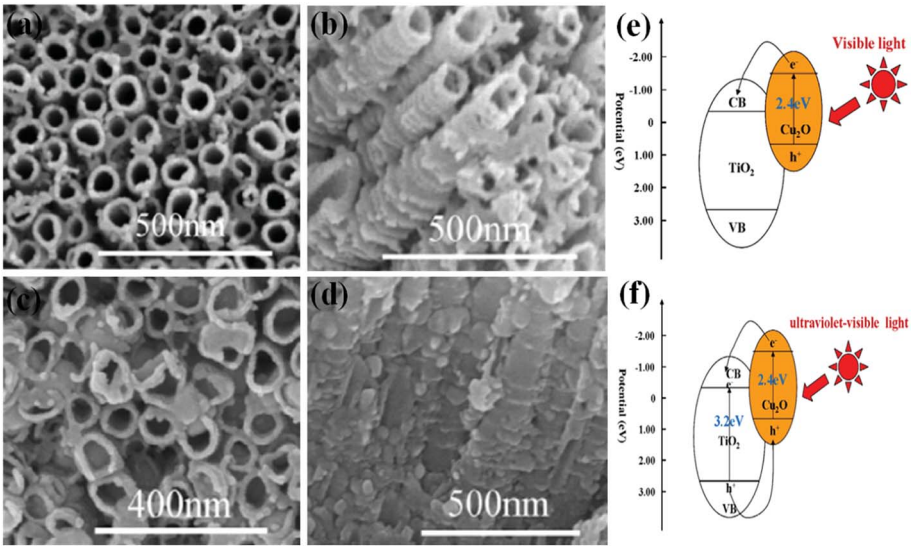

Fig. 11 SEM images of (a and b) TiO_2 NTs and (c and d) Cu_2O/TiO_2 NT heterojunction; schematic of the charge separation of Cu_2O/TiO_2 NT heterojunction structure under (e) visible light and (f) UV-vis light irradiations. Reproduced from ref. 149 with permission from Elsevier.

CuO and TiO_2 was characterized by HRTEM, and the HRTEM image is shown in Fig. 12a. The typical monoclinic CuO {110} and anatase TiO_2 {101} planes with the characteristic lattice spacing of 0.275 nm and 0.35 nm were observed, respectively. A surface-phase heterojunction existed between CuO and TiO_2, and the band position of CuO and TiO_2 is shown in Fig. 12b. This heterojunction can improve charge migration and accelerate the separation of e^-/h^+ pairs, enhancing the photocatalytic performance.

A series of Cu (Cu^0, Cu^I, Cu^{II})/TiO_2 photocatalysts *via* an improved impregnation method through the reduction–oxidation steps was fabricated by Gunlazuardi *et al.*[158] The 3 wt% CuO/TiO_2 exhibited the highest CH_3OH yield (~442.5 μmol g^{-1} h^{-1}), which was 3.28, 2.28, and 1.97 times higher than TiO_2 (134.8 μmol g^{-1} h^{-1}), 3 wt% Cu/TiO_2 (194 μmol g^{-1} h^{-1}), and 3 wt% Cu_2O/TiO_2 (224.3 μmol g^{-1} h^{-1}), respectively. It was clearly indicated that CuO was the main dopant species that enhanced the CH_3OH yield. In a further study, Wilkinson *et al.* also reported CuO loaded onto TiO_2 hollow microspheres by a one-pot template-free strategy.[159] Further, it exhibited a higher CH_4 formation rate than commercial Degussa P25 due to its large surface area, which contributed toward the adsorption of CO_2 and offered a large number of active sites.

In *et al.* synthesized hybrid Cu_xO–TiO_2 ($x = 1, 2$) mesoporous heterojunction photocatalysts by two steps, and the synthesis process is shown in Fig. 13a.[160] Initially, hybrid mesoporous Cu_xO/TiO_2 heterojunctions for the photocatalytic reduction of CO_2 into solar fuels were reported. CT07 ($TiCl_4$ was 0.7 mL mixed with the dispersion liquid of Cu/Cu_2O nanocomposites) had a higher CH_4 formation rate (221.63 ppm g^{-1} h^{-1}) than CuO and TiO_2 due to the enhanced light absorption and rapid charge separation. The charge transfer of Cu_xO–TiO_2 heterojunction is shown in Fig. 13b. Here, e^- could transfer from the CB of Cu_xO to TiO_2 and react with CO_2 to produce CH_4. Schaak

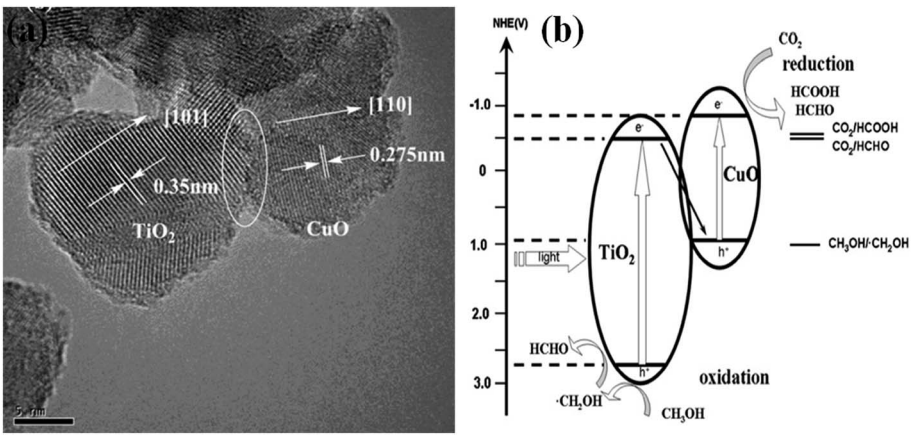

Fig. 12 (a) HRTEM image of CuO/TiO_2 NTs; (b) schematic of the charge separation of CuO/TiO_2 NT heterojunction. Reproduced from ref. 157 with permission from Elsevier.

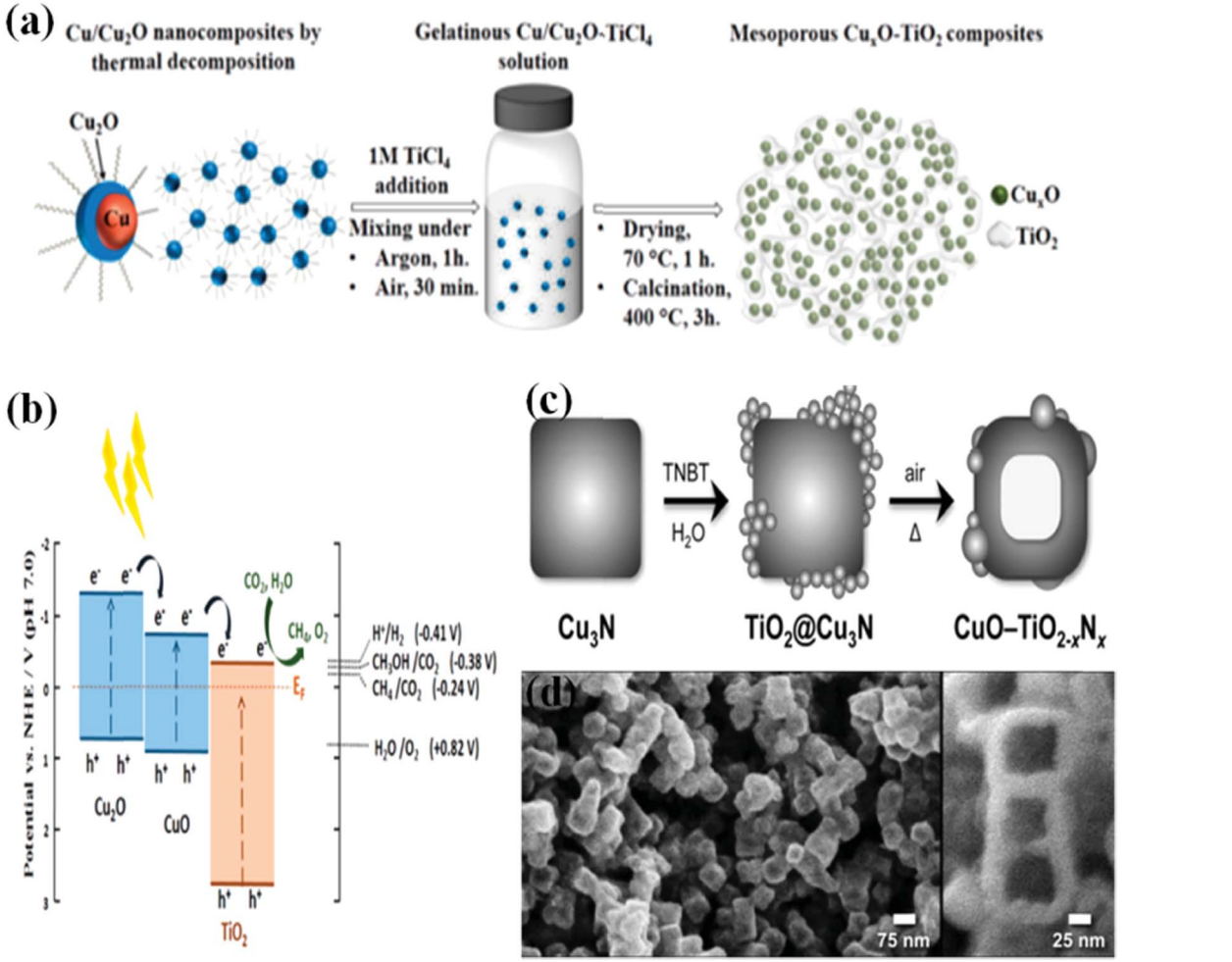

Fig. 13 (a) Schematic view of the synthesis of mesoporous Cu_xO–TiO_2 photocatalysts; (b) schematic of the charge transfer in the Cu_xO–TiO_2 heterojunction; (c) schematic view of the synthesis of CuO–$TiO_{2-x}N_x$ hollow nanocubes; (d) FESEM images of the CuO–$TiO_{2-x}N_x$ hollow nanocubes. (a and b) Reproduced from ref. 160 with permission from the American Chemical Society. (c and d) Reproduced from ref. 161 with permission from Wiley-VCH.

et al. reported novel hollow CuO nanocubes loaded over titanium oxynitride ($TiO_{2-x}N_x$) by a multi-template strategy (Fig. 13c).[161] Fig. 13d shows the FESEM images of the CuO–$TiO_{2-x}N_x$ hollow nanocubes. N doped onto TiO_2 could extend the light absorption capability into the visible light region. The photocurrent density of a thin film of CuO–$TiO_{2-x}N_x$ under AM 1.5G irradiation could confirm the formed p–n heterojunction by electrochemical evidence. The CuO–$TiO_{2-x}N_x$ hollow nanocubes exhibited a higher CH_4 production rate (41.3 ppm g^{-1} h^{-1}) than Degussa P25 (16.2 ppm g^{-1} h^{-1}).

In a previous work, GaP was used for the photoelectrochemical reduction of CO_2 in 1978. However, it is rarely used as a photocatalyst owing to the low oxidizing power of its VB.[162] Here, e^- in the CB can convert CO_2 into CH_4, but h^+ in the VB is unable to oxidize H_2O; therefore, bare GaP cannot induce the photocatalytic reduction of CO_2. GaP coupled with TiO_2 that forms a p–n heterojunction for the photocatalytic reduction of CO_2 was fabricated by Marcì *et al.* for the first time.[163] GaP/TiO_2 composites could effectively exhibit both the reduction of CO_2 and oxidation of H_2O, and the p–n heterojunction could promote the separation of e^-/h^+ pairs. The highest photocatalytic performance was obtained with 10 wt% GaP, which was ascribed to the band structures and charge transfer between GaP and TiO_2.

4.1.2 Non-p–n heterojunction. Non-p–n heterojunction is another type of heterojunction. Owing to the staggered alignment of the energy levels, non-p–n heterojunction structures have been already used for promoting the performance of the photocatalytic reduction of CO_2 into solar fuels.

In previous studies, sulfide semiconductors have received considerable attention. Furthermore, many sulfides (*e.g.*, CdS, PbS) have a narrow bandgap, where the onset of absorption begins in the visible light or even infrared region. However, heavy metal ions, *e.g.*, Pb(II), Hg(II), Cr(VI), and Cd(II), exhibit obvious non-biodegradation and bioaccumulation and cannot easily degrade into cleaner products, which cause severe water pollution and induce serious threats to living organisms.[164–167] Moreover, bare sulfide semiconductors exhibit photocorrosion.

Recent studies have confirmed that sulfide semiconductors are promising materials for the photosensitization of TiO_2 in the photocatalytic reduction of CO_2.[168] Coupling with TiO_2 to form a heterojunction can both overcome the photocorrosion of sulfide semiconductors and improve the photocatalytic activity of TiO_2. Yin *et al.* synthesized the CdS/TiO_2 heterojunction *via* two-step hydrothermal methods, and its synthesis process is shown in Fig. 14a.[169] Fig. 14b and c show the TEM images of TiO_2 nanosheets and CdS/TiO_2 heterojunction composites. The sizes of the TiO_2 nanosheet were about 50–60 nm. The HRTEM image of the CdS/TiO_2 heterojunction composite is shown in Fig. 14d, where the typical crystallized cubic CdS {002} and anatase TiO_2 {010} planes with the characteristic lattice spacing of 0.334 nm and 0.378 nm, respectively, were observed.[170] The CdS NPs were dispersed on the surface and edge of the TiO_2 nanosheet, and the interface could form a non-p–n heterojunction. Cyclohexanol was used as the solvent and reductant because the solubility of CO_2 in cyclohexanol was much higher than that in water at room temperature. With the optimum molar ratio of TiO_2 to CdS (8 : 1), it exhibited the maximum cyclohexyl formate (CF) yield. The band energy values and charge carrier transfer of CdS/TiO_2 are shown in Fig. 14e. The high separation and transfer of e^-/h^+ pairs in this heterojunction were crucial for its high photocatalytic activity.

A similar finding about CdS/TiO_2 for the photocatalytic reduction of CO_2 was reported by Fatemi *et al.*[171] Here, 45% CdS/TiO_2 exhibited the maximum CO and CH_4 formation rates under both UV-vis and visible light irradiations. In another work, Li *et al.* reported the CdS or Bi_2S_3 loaded onto TiO_2 NTs *via* a direct precipitation method.[172] The CH_3OH yields of CdS/TiO_2 and Bi_2S_3/TiO_2 were about 159.5 and 224.6 μmol L^{-1}, respectively, which were higher than those of P25 (91 μmol L^{-1}) and TiO_2 NTs (102.5 μmol L^{-1}). The loaded CdS or Bi_2S_3 could improve the visible light absorption and photocatalytic activity. The different sizes of PbS quantum dots (QDs) loaded onto TiO_2 for the photocatalytic reduction of CO_2 was reported by Wang *et al.*[173] It was interesting to note that 4 nm PbS-QD-sensitized TiO_2 yielded a higher CO_2 conversion rate than the 3 and 5 nm counterparts because of the synergetic effects of good light absorption and high charge separation properties. In particular, the decreased activity with larger particles was attributable to the smaller surface areas and longer electron migration paths, whereas the decreased activity with smaller particles was associated with changes in the optical and electronic properties.

Zhao *et al.* synthesized CeO_2 loaded onto 3D ordered macroporous (3DOM) TiO_2 *via* the gas bubbling-assisted membrane precipitation (GBMP) method.[174] The SEM images of 3DOM TiO_2 and CeO_2/TiO_2 are shown in Fig. 15a and b, respectively. From Fig. 15a, it is evident that 3DOM TiO_2 had periodic voids, where the average diameter and wall thickness were about 310 ± 10 nm and 40 ± 5 nm, respectively. After the loading of CeO_2, the morphology did not obviously change. The result of UV-vis DRS indicated that 3DOM CeO_2/TiO_2 had a good photoresponse from the UV to the visible light region. 3DOM CeO_2/TiO_2 possessed high photocatalytic activity. The mechanism for the enhanced activity of 3DOM CeO_2/TiO_2 is shown in Fig. 15c. In a similar study by Wang *et al.*, the mesoporous CeO_2/TiO_2 photocatalyst with a 2D hexagonal structure was synthesized *via*

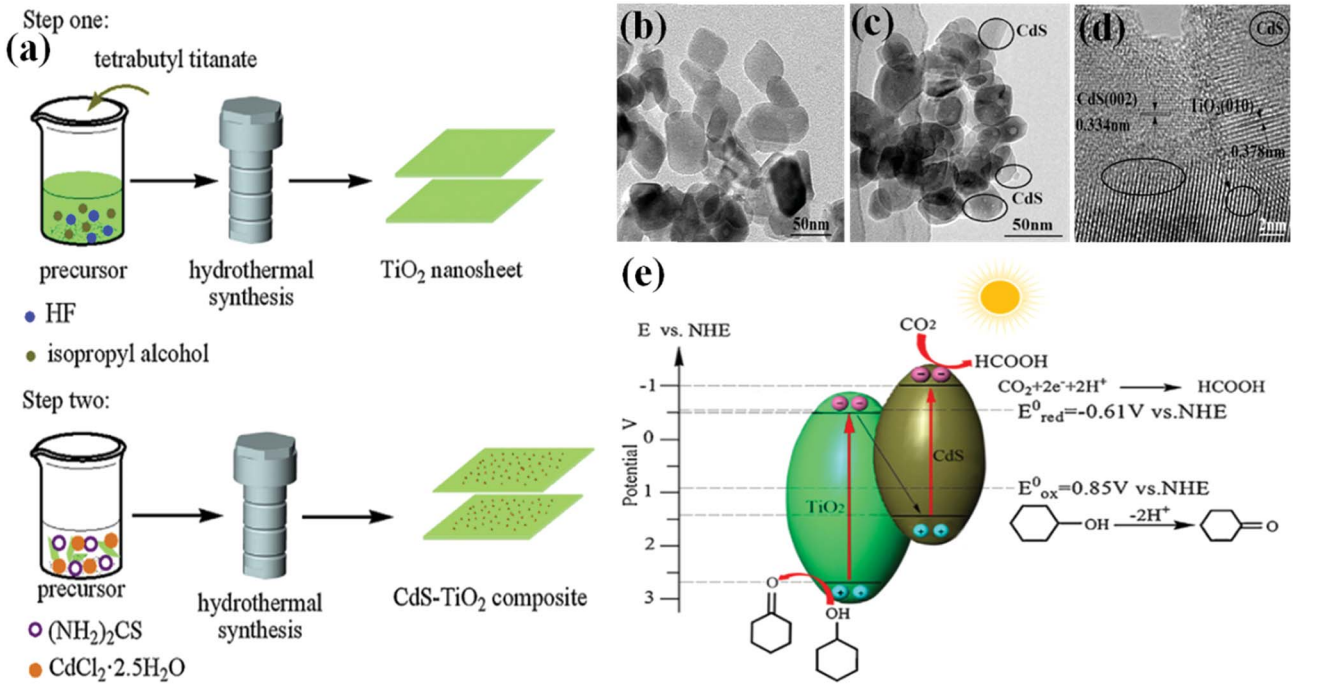

Fig. 14 (a) Schematic view of the synthesis of CdS–TiO_2 composites; TEM images of (b) TiO_2 nanosheets and (c) CdS–TiO_2 composites; (d) HRTEM image of CdS–TiO_2 composite; (e) band energy values and charge carrier transfer of CdS/TiO_2 composites. Reproduced from ref. 169 with permission from Elsevier.

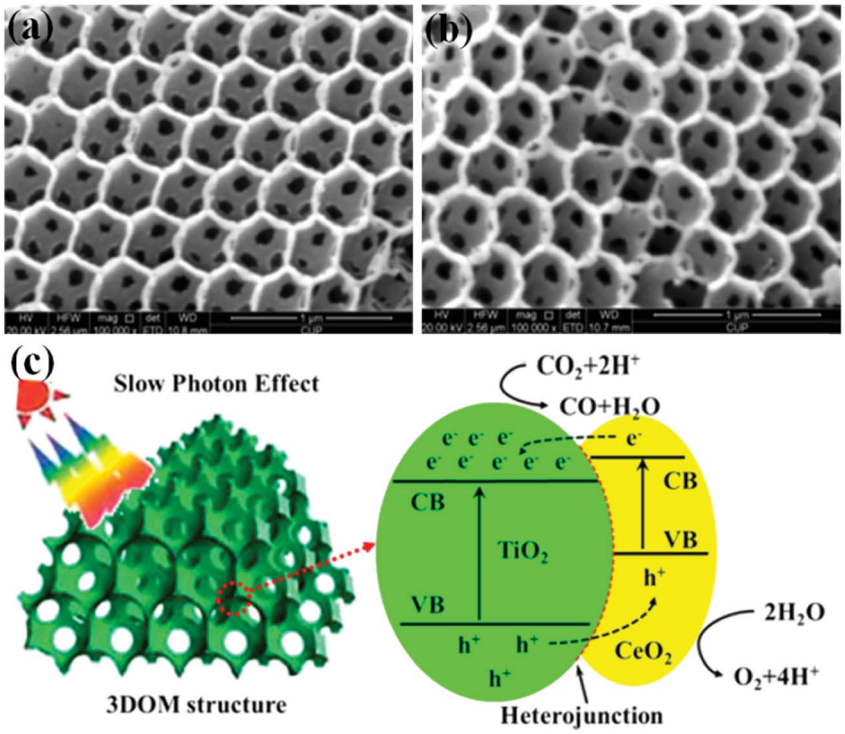

Fig. 15 SEM images of (a) 3DOM TiO_2 and (b) CeO_2–TiO_2; (c) mechanism for the enhanced activity of 3DOM CeO_2/TiO_2. Reproduced from ref. 174 with permission from the American Chemical Society.

a nanocasting method.[175] Its photocatalytic activity was much higher than that of commercial P25.

When compared with sulfides, many oxides do not undergo photooxidation under light irradiation and have been widely used in photocatalytic reduction and oxidation processes. For example, zinc oxide (ZnO) is an n-type semiconductor with a direct bandgap (~3.3 eV), and it is usually used in photocatalytic oxidation processes.[176] ZnO hybrid photocatalysts have aroused considerable attention due to its high effective separation of e^-/h^+ pairs. Ye *et al.* synthesized TiO_2/ZnO mesoporous "French fries" (MFFs) hybrid photocatalyst *via* a facile furfural alcohol-derived polymerization–oxidation (FAPO) method.[177] The CH_4 formation rate over TiO_2/ZnO MFFs was 55 μmol g^{-1} h^{-1}, which was 5.9 times higher than that of commercial P25 (9.3 μmol g^{-1} h^{-1}). In another work, Wu *et al.* reported V and W doped onto TiO_2 and then coated onto a honeycomb support.[178] After doping with V and W, the visible light absorption and charge separation improved. V_2O_5 and TiO_2 could form a heterojunction and doping W^{6+} could trap e^- and react with CO_2 and H_2O to yield solar fuels. Therefore, the photocatalytic activity was improved.

$FeTiO_3/TiO_2$ heterojunction photocatalysts were synthesized by Ling *et al.*[179] The highest CH_3OH yield of 10% $FeTiO_3/TiO_2$ was 0.462 μmol g^{-1} h^{-1} and 0.432 μmol g^{-1} h^{-1} under UV-vis and visible light irradiations, respectively. Due to the unique band structure and heterojunction over $FeTiO_3/TiO_2$, the CH_3OH yield was obviously improved. Ye *et al.* reported $SrTiO_3$ (STO) loaded onto TiO_2 NT arrays (TNA) *via* a facile hydrothermal method and then Au–Cu bimetallic alloys were loaded on the STO/TNA *via* the microwave-assisted solvothermal route.[180] The Au_3Cu@STO/TNA exhibited good photocatalytic activity for the generation of CO and CH_4 under UV-vis light irradiation. Owing to the alloying effect, the Au–Cu alloy yielded higher activity than that of pure Au and Cu. STO and TiO_2 could form a heterojunction to facilitate photogenerated carrier separation.

Graphitic carbon nitride (g-C_3N_4) with a moderate bandgap energy (~2.7–2.8 eV) has aroused considerable attention for photocatalytic applications in the last couple of years. However, its photocatalytic activity is very low because of the high recombination of charge carriers. Various methods, such as using a heterojunction, have been investigated to enhance the photocatalytic activity of g-C_3N_4. Reli *et al.* synthesized TiO_2/g-C_3N_4 *via* the simple mechanical mixing of g-C_3N_4 with TiO_2.[181] Further, (0.3/1) TiO_2/g-C_3N_4 showed good photocatalytic activity for the photocatalytic reduction of CO_2 to produce CH_4 and CO. In a similar work, Zhao *et al.* tuned the mass ratios of urea and $Ti(SO_4)_2$ to synthesize g-C_3N_4–N-TiO_2 heterojunction catalysts.[182] It was interesting to find that CO was the main product of the g-C_3N_4–N-TiO_2 heterojunction, whereas CH_4 and CO were the main products of N-TiO_2. Therefore, the g-C_3N_4 could suppress CH_4 formation.

Recently, colorful inorganic materials with high stability and strong absorption in the visible light region have been used for modifying TiO_2. AgBr often serves as a photosensitive material to improve the activity. He *et al.* reported the AgBr/TiO_2 photocatalyst for CO_2 reduction to CH_4, CH_3OH, CH_3CH_2OH and CO under visible light irradiation.[183] It was interesting to find

that 23.2% AgBr/TiO_2 exhibited the maximum yield and high stability.

4.1.3 Z-scheme heterojunction. Lately, another Z-scheme heterojunction system has been developed for the photocatalytic reduction of CO_2.[184,185] Gondal *et al.* first synthesized a direct Z-scheme Si/TiO_2 *via* a hydrothermal method.[186] The direct Z-scheme Si/TiO_2 exhibited better photocatalytic performance for the photocatalytic reduction of CO_2 into CH_3OH than that of individual Si and TiO_2, because this Z-scheme system could considerably enhance the separation efficiency of e^-/h^+ pairs and prolong their longevity. In another report, Xin *et al.* fabricated $ZnFe_2O_4/TiO_2$ nanobelts Z-scheme heterojunction photocatalyst *via* two-step hydrothermal methods.[187] The obtained $ZnFe_2O_4/TiO_2$ exhibited high photocatalytic performance in cyclohexanol for the photocatalytic reduction of CO_2 under UV light irradiation. Furthermore, the introduction of $ZnFe_2O_4$ could extend the response of TiO_2 into the visible light region.

The all-solid-state Z-scheme CdS/reduced graphene oxide (rGO)/TiO_2 core–shell nanostructure for the photocatalytic reduction of CO_2 into CH_4 was reported by Zou *et al.*, where rGO served as the electron mediator to accelerate the separation of e^-/h^+ pairs and improve the stability of CdS.[188] The charge transfer in CdS/rGO/TiO_2 Z-scheme heterojunction system is shown in Fig. 16. Under UV-vis light irradiation, both CdS and TiO_2 could produce e^- and h^+. As the CB of TiO_2 was negative than the Fermi level of rGO, e^- could transfer from the CB of TiO_2 to rGO and then recombine with h^+ in the VB of CdS. This process effectively improved h^+ in TiO_2 for the oxidation of H_2O and e^- in CdS for the photocatalytic reduction of CO_2.

4.2 TiO_2–metal heterojunction

Metals and semiconductors have different physical and chemical properties. When they couple with each other, a heterojunction (Schottky barrier) is produced, which can produce a space–charge separation region.[136] The Schottky barrier also works as an electron trap to reduce the recombination of e^-/h^+ pairs. Further, n-type semiconductors, such as TiO_2, usually form this heterojunction. Moreover, the work function of a metal is often higher than that of TiO_2. A metal can also produce e^- by the localized surface plasmon resonance (SPR) excitation under light irradiation. The schematic of TiO_2–metal heterojunction is shown in Fig. 17.[136] Here, e^- can flow from TiO_2 to the metal in order to align the Fermi energy levels. Therefore, metal and TiO_2 are excessively negative and positive, respectively. Further, e^- can aggregate in the CB of TiO_2 and react with CO_2 and H^+ to produce solar fuels; h^+ in the VB of TiO_2 reacts with H_2O to generate H^+ and O_2. Table 4 summarizes and compares the typical TiO_2–metal heterojunction photocatalysts for the photocatalytic reduction of CO_2.

The activation of CO_2 is more efficiently performed on TiO_2 decorated with noble-metal NPs. Zhao *et al.* prepared uniform Au NPs supported on 3DOM TiO_2 *via* a facile GBMR method.[189] Fig. 18A shows the UV-vis DRS of P25, 3DOM TiO_2, and 3DOM Au/TiO_2. It was clearly observed that 3DOM TiO_2 exhibited a slight red-shift in comparison with P25, and 3DOM Au/TiO_2 had a broad band centered by the Au SPR effect.[190] It was interesting to find that increasing the Au amounts could remarkably improve the visible light absorbance. Fig. 18B shows the CH_4 production amount under visible light irradiation. The 3DOM Au_8/TiO_2 exhibited the highest CH_4 formation rate (2.89 μmol g^{-1} h^{-1}), which was 2.61 and 2.03 times higher than those of P25 (1.11 μmol g^{-1} h^{-1}) and 3DOM TiO_2 (1.42 μmol g^{-1} h^{-1}), respectively. The photocatalytic mechanism of 3DOM Au/TiO_2 is shown in Fig. 18C. The 3DOM TiO_2 structure could increase the light absorption and diffusion of CO_2, and Au also extended the spectral range from the UV to the visible light region.

Charge recombination is an important negative effect on the photocatalytic performance. Chai *et al.* synthesized Ag-doped multiwalled carbon nanotubes (MWCNT)@TiO_2 core–shell photocatalysts *via* a one-step method with the core–shell coating approach, where MWCNT and TiO_2 served as the core and shell, respectively.[191] The HRTEM image of Ag-doped MWCNT@TiO_2 (Fig. 19a) showed the Ag–TiO_2 heterojunction. In Fig. 19b, the CH_4 formation rate was evaluated with respect to the photocatalytic activity. It was revealed that the Ag-doped MWCNT@TiO_2 had good stability and 2 wt% Ag doping exhibited the highest CH_4 formation rate under visible light irradiation. Fig. 19c shows the charge transfer route in Ag-MWCNT@TiO_2. Further, e^- could transfer to the MWCNT and

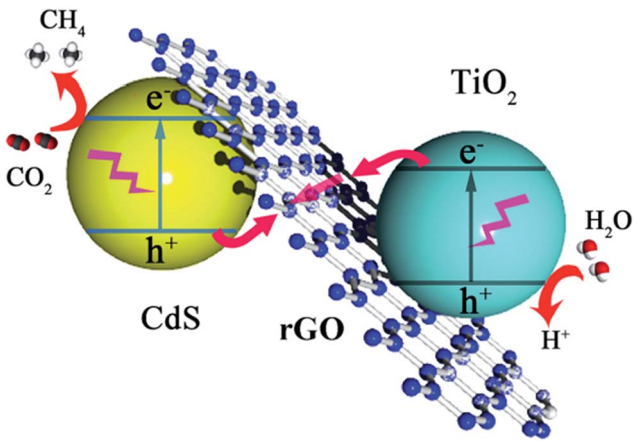

Fig. 16 Schematic of CdS/rGO/TiO_2 Z-scheme system. Reproduced from ref. 188 with permission from The Royal Society of Chemistry.

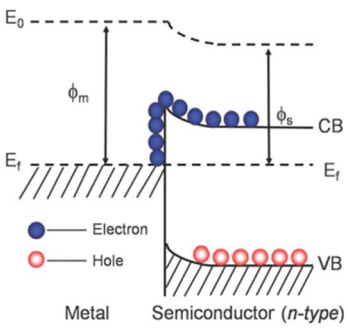

Fig. 17 Schematic of a Schottky barrier. Reproduced from ref. 136 with permission from The Royal Society of Chemistry.

Table 4 Comparison of typical TiO_2–metal heterojunction systems

Photocatalyst	Solvent	Light source	Time[a]	Formation rate[b]	QE[c] (%)	Reference
3DOM Au/TiO_2	H_2O	Xe lamp	8	CH_4: 2.89	—	189
Ag-MWCNT@TiO_2	H_2O	Energy saving light	7.5	CH_4: 0.91; C_2H_4: 0.048	—	191
CdSe/Pt/TiO_2	H_2O	Xe lamp (λ > 420 nm)	6	CH_4: 48 ppm g^{-1} h^{-1}	—	193
RGO/Pt–TiO_2 NTs	H_2O	Tungsten halogen lamp	5	CH_4: 2.88 μmol m^{-2} h^{-1}	—	194

[a] Irradiation time, h. [b] Formation rate, μmol g^{-1} h^{-1}. [c] Quantum efficiency (%).

Ag to reduce the recombination rate of e^-/h^+ pairs, improving the photocatalytic performance.

It has been reported that semiconductor nanocrystal QDs that can sensitize TiO_2 can make full use of the visible light spectrum and increase charge separation efficiency.[192] Wang *et al.* synthesized Pt/TiO_2 *via* a wet impregnation method and then CdSe QDs were assembled on Pt/TiO_2.[193] Under visible light irradiation, CdSe/Pt/TiO_2 exhibited a high CH_4 formation rate. In another study, Saravanan *et al.* reported rGO loaded onto Pt/TiO_2 NTs for CO_2 reduction under visible light irradiation. Pt NPs could increase the visible light absorption by the LSPR effect and rGO could be used as an electron reservoir to reduce the recombination rate of e^-/h^+ pairs.[194]

4.3 TiO_2–carbon heterojunction

GR is a new class of material in carbon atoms, which has a two-dimensional sp^2-hybridized carbon atom in the carbon family.[195–198] It has some unique properties, such as high surface area (2600 m^2 g^{-1}),[199–202] high thermal conductivity (5000 W m^{-1} K^{-1}),[203,204] high mobility of charge carriers (200 000 cm^2 V^{-1} s^{-1}),[205,206] and good optical transparency (97.7%).[207] It was first prepared by Novoselov *et al.*;[208] it has received increased attention due to its potential applications. Furthermore, GR can also improve the separation of e^-/h^+ pairs and suppress the recombination of e^-/h^+ pairs. Table 5 summarizes and compares the typical TiO_2–carbon heterojunction photocatalysts for the photocatalytic reduction of CO_2.

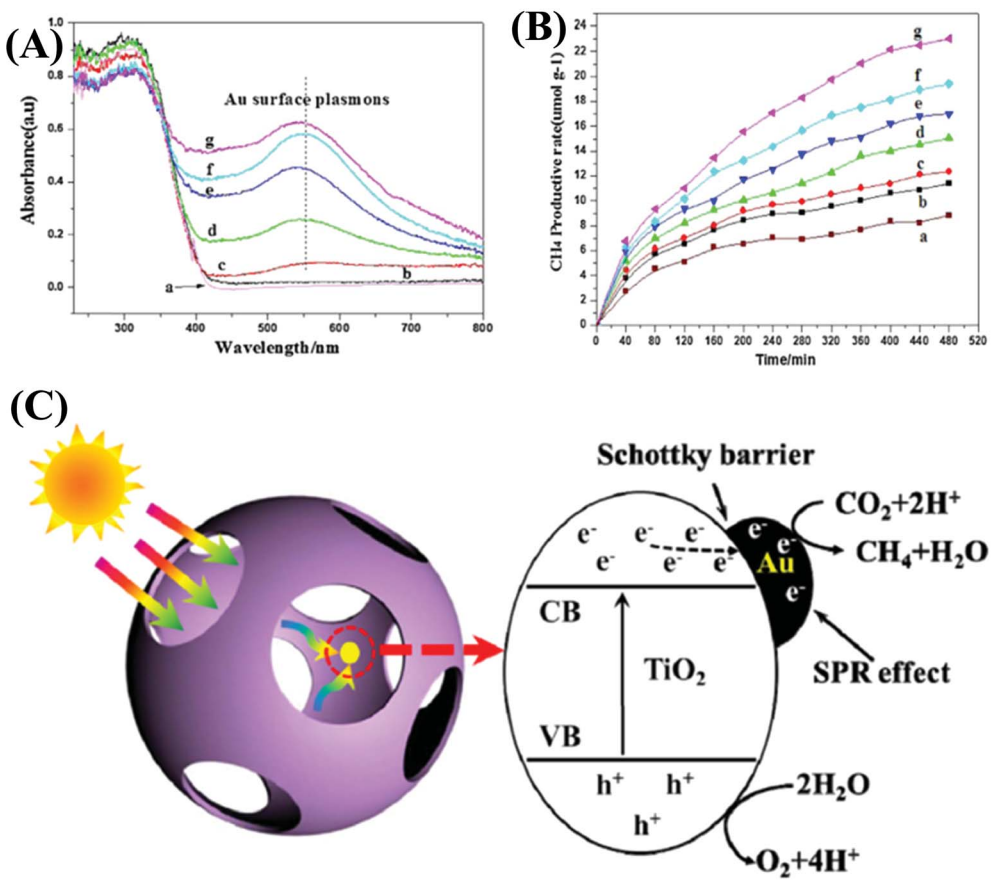

Fig. 18 (A) UV-vis DRS of 3DOM Au/TiO_2; (B) CH_4 production amounts of 3DOM Au/TiO_2; (C) possible photocatalytic mechanism of 3DOM Au/TiO_2. (a) P25; (b) TiO_2; (c) $Au_{0.5}/TiO_2$; (d) Au_1/TiO_2; (e) Au_2/TiO_2; (f) Au_4/TiO_2; (g) Au_8/TiO_2. Reproduced from ref. 189 with permission from Elsevier.

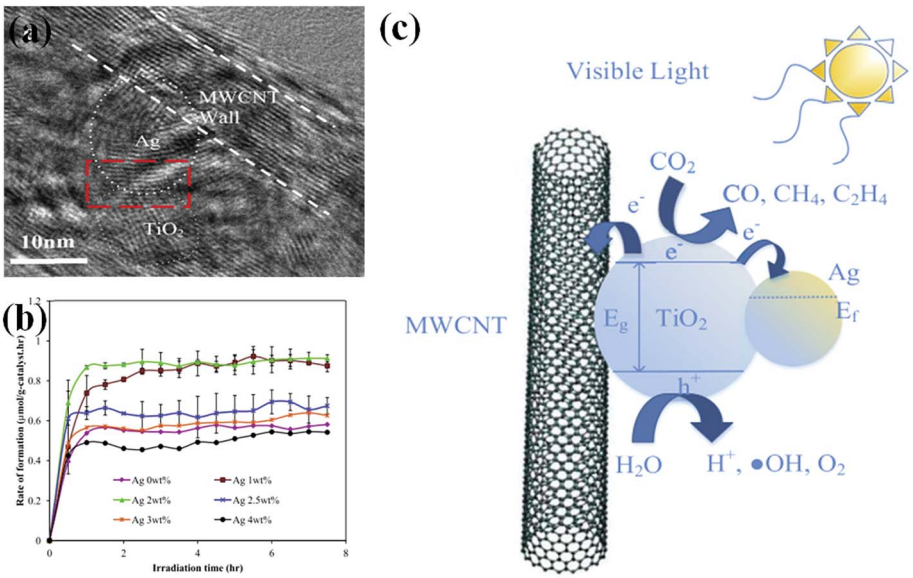

Fig. 19 (a) HRTEM image of 2 wt% Ag-MWCNT@TiO_2; (b) CH_4 formation rate over Ag-MWCNT@TiO_2; (c) schematic of charge transfer in Ag-MWCNT@TiO_2. Reproduced from ref. 191 with permission from Elsevier.

The Cu_2O/GR/TNA heterostructure for the photocatalytic reduction of CO_2 under visible light irradiation was reported by Cao *et al.*[209] The fabrication steps for the Cu_2O/GR/TNA heterostructure is shown in Fig. 20a. TNA was first synthesized by two-step anodization methods on Ti foils and then GR was loaded by cyclic voltammetric reduction. Lastly, Cu_2O was loaded by an electrochemical deposition method. It was found that the highest CH_3OH yield was achieved by the Cu_2O/GR/TNA heterostructure (Fig. 20b). Under visible light irradiation, e^- and h^+ were produced by Cu_2O. With the help of GR, e^- could transfer to the CB of TNA; therefore, e^- and h^+ were effectively separated. The possible mechanism of Cu_2O/GR/TNA is proposed in Fig. 20c. The ternary heterojunction could increase the visible light absorption and suppress the recombination of e^-/h^+ pairs. In a similar study, Chai *et al.* reported N-doped TiO_2 with exposed {001} facet (N-TiO_2-001) loaded onto GR sheets to fabricate the N-TiO_2-001/GR catalyst *via* the solvothermal method.[210] The N-TiO_2-001/GR showed the highest photocatalytic activity due to the high catalytic activity of {001} facet and GR.

Graphene oxide (GO) is a ramification of GR, which has abundant oxygenated functional groups (*e.g.*, –OH, –COOH) on its surface and large surface area.[211–213] Moreover, we often use GO as the precursor to fabricate GR–semiconductor composite photocatalysts.[214–216] Under chemical or thermal conditions, GO can be readily reduced to GR, which is commonly referred to as rGO.[217] The rGO–TiO_2 hybrid photocatalyst was synthesized by Chai *et al. via* a solvothermal method.[218] rGO–TiO_2 had a high CH_4 formation rate (0.135 μmol g^{-1} h^{-1}) under visible light irradiation. The intimate interface between rGO and TiO_2 largely improved the transfer of e^- from TiO_2 to rGO, resulting in the enhanced CH_4 formation rate. In a further study, Chai *et al.* synthesized GO-doped O-rich TiO_2 (GO–OTiO_2) heterojunction structure *via* a chemical impregnation method.[219] It was found that 5 wt% GO–OTiO_2 yielded the highest CH_4 formation rate (0.29 μmol g^{-1} h^{-1}) and good photostability. In another report, noble metals (Pt, Pd, Ag, and Au) loaded onto rGO/TiO_2 (GT) were also synthesized by Chai *et al.*, where Pt achieved the highest CH_4 yield among these noble metals.[220] The photocatalytic performance was strongly related to the work function of the metal, where Pt had the highest work function and e^- could effectively transfer from TiO_2 to Pt. The possible mechanism of Pt–GT for the photocatalytic reduction of CO_2 to CH_4 is shown in Fig. 21. Under light irradiation, TiO_2 could

Table 5 Comparison of typical TiO_2–carbon heterojunction systems

Photocatalyst	Solvent	Light source	Time[a]	Formation rate[b]	QE[c] (%)	Reference
Cu_2O/graphene/TiO_2 NTs	1 M $NaHCO_3$	Xe lamp	6	CH_3OH: 45 μmol cm^{-2} h^{-1}	—	209
N-TiO_2-001/GR	H_2O	Energy-saving lamp	10	CH_4: 0.37	—	210
rGO–TiO_2	H_2O	Energy-saving bulb	5	CH_4: 0.135	—	218
GO–OTiO_2	H_2O	Energy-saving bulb	6	CH_4: 0.29	—	219
Pt–rGO–TiO_2	H_2O	Energy-saving bulb	6	CH_4: 0.28	—	220
N-CQDs–TiO_2	H_2O	Xe lamp	6	CH_4: 3.98; CO: 6.13	—	223

[a] Irradiation time, h. [b] Formation rate, μmol g^{-1} h^{-1}. [c] Quantum efficiency (%).

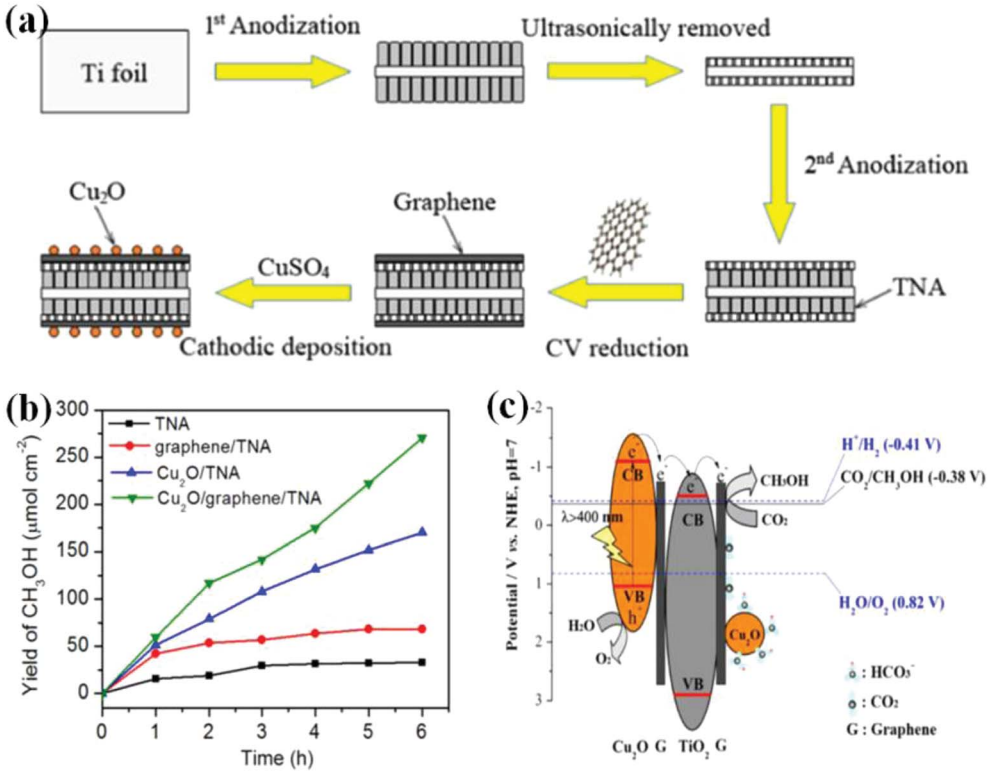

Fig. 20 (a) Fabrication steps for Cu_2O/GR/TNA heterostructure; (b) photocatalytic CH_3OH evolution over 6 h for Cu_2O/GR/TNA heterostructure; (c) possible mechanism of Cu_2O/GR/TNA. Reproduced from ref. 209 with permission from Elsevier.

produce e^- and h^+. Moreover, Pt could effectively trap e^- to react with CO_2 and H^+ to produce CH_4 (path 1). Furthermore, Pt was also deposited onto rGO sheets. Therefore, e^- could pass the two-dimensional carbon network to rGO sheets and then get trapped by the Pt sites to react with CO_2 and H^+ (path 2).

Carbon quantum dots (CQDs) are a new class of material in the carbon family, which exhibit good efficiency of charge separation and electron reservoir properties.[221] These CQDs can absorb visible and near-infrared (NIR) light in the solar spectrum.[222] Therefore, coupling CQDs with TiO_2 can ensure full use of the solar spectrum. Cao *et al.* reported N-CQDs/TiO_2 heterojunctions for the photocatalytic reduction of CO_2.[223] CH_4 and CO were the major products under simulated solar light irradiation. These N-CQDs could serve as the photosensitizer and electrons reservoir to enhance the photocatalytic activity.

4.4 Phase or facet TiO_2 heterojunction

4.4.1 Phase heterojunction. The phase heterojunction structure only exists in one semiconductor with two or more different crystal phases. Recently, the phase heterojunction has attracted considerable attention for the photocatalytic reduction of CO_2.[224–226] TiO_2 has the anatase, brookite, and rutile phases. Anatase-based catalysts usually have high activity when compared with rutile-based catalysts owing to the fast recombination of e^-/h^+ pairs in the rutile phase. Further, brookite-based catalysts are rarely studied because it is very difficult to synthesize high-purity brookite.[227] Table 6 summarizes and compares the typical phase or facet of TiO_2 heterojunction photocatalysts for the photocatalytic reduction of CO_2.

Bai *et al.* reported that anatase TiO_2 nanorods (TiO_2–RMA) with the {010} facet modified with rutile TiO_2 NPs were synthesized *via* a one-step method.[228] The HRTEM image of TiO_2–RMA is shown in Fig. 22a. The clear lattice fringes with a *d*-spacing of 0.32 nm and 0.35 nm for the rutile {110} and anatase {101} facets, respectively, were identified. Rutile–anatase heterojunction showed high CH_4 formation rate (2.36 μmol g^{-1} h^{-1}) under UV light irradiation, and the possible mechanism is shown in Fig. 22b. Due to the fact that the CB of anatase was more negative than that of rutile, e^- could transfer from anatase to rutile. Therefore, e^- and h^+ could be effectively separated. In a similar study, Gray *et al.* used the structure–function understanding to fabricate anatase–rutile TiO_2 phases for the photocatalytic reduction of CO_2, and high selectivity toward CH_4 was obtained.[229] Gray *et al.* used the direct current (DC) magnetron sputtering to synthesize mixed-phase TiO_2 films (70% anatase and 30% rutile).[230] In another report, Zhao *et al.* synthesized Au–Pd bimetallic metal loaded onto 3DOM TiO_2 with the anatase–rutile phases.[231] The Au_3Pd_1/3DOM TiO_2 exhibited the maximum CH_4 formation rate (18.5 μmol g^{-1} h^{-1}) because the Au–Pd bimetallic metal had a relatively low Fermi level than that of TiO_2 and the separation of e^-/h^+ pairs was accelerated.

The anatase, brookite, and rutile phases of TiO_2 can be accurately tuned by the solution's pH. For example, Ling *et al.* synthesized anatase–brookite mixed phases *via* a facile hydrothermal method.[232] The TEM image of anatase–brookite TiO_2 is

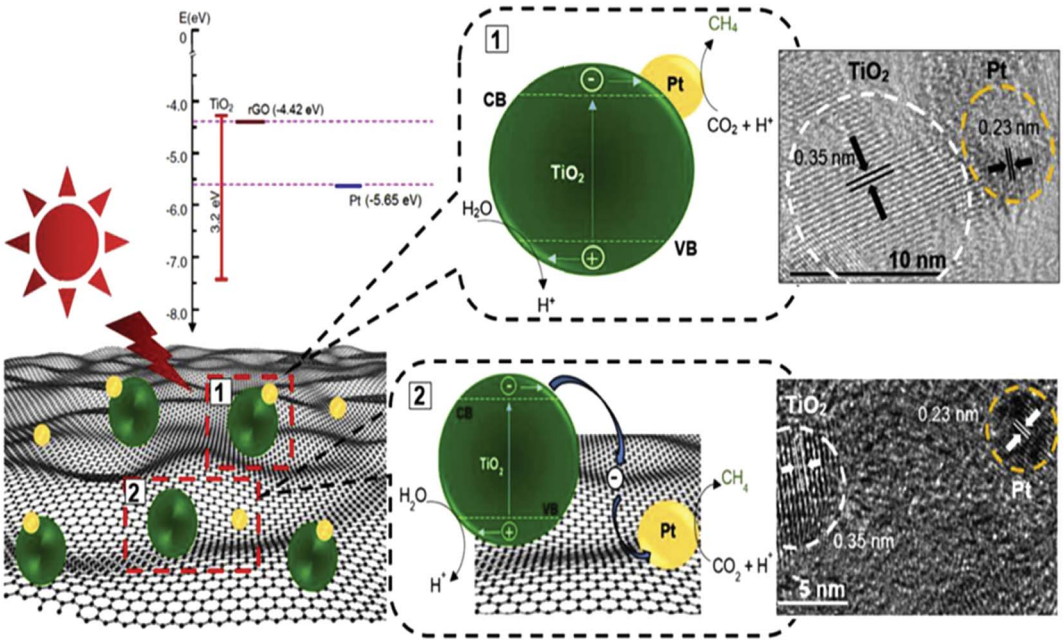

Fig. 21 Possible mechanism of Pt–GT composite. Reproduced from ref. 220 with permission from Elsevier.

shown in Fig. 23a. It was indicated that rod-like and spherical NPs were the typical structures of the brookite and anatase phases, respectively.[233] Anatase–brookite TiO_2 exhibited the highest CH_3OH formation rate under both UV-vis and visible light irradiations. The charge transfer between anatase–brookite TiO_2 is shown in Fig. 23b. Here, e^- could transfer from the CB of brookite to anatase to react with CO_2 and H^+ for the production of CH_3OH, and h^+ could transfer from the VB of anatase to brookite to react with H_2O to produce O_2 and H^+. Li *et al.* also reported that the anatase–brookite mixed-phase TiO_2 showed the highest CO yield for the photocatalytic reduction of CO_2 when compared with single-phase anatase and brookite TiO_2 and P25.[234]

4.4.2 Facet heterojunction. Recent studies have confirmed that exposed facets play a critical role in improving the photocatalytic performance. On account of the first-principles calculations, the {101} facet of anatase TiO_2 is the primary CO_2 adsorption site for CO_2 reduction.[235] Moreover, the {101} facet can accelerate e^- transfer from the surface of TiO_2 to CO_2. Yu *et al.* first controlled the ratio of coexposed {001} and {101} facets of anatase TiO_2 for the photocatalytic reduction of CO_2 to CH_4.[235] Fig. 24a shows the schematic involving the tuning of the {001} and {101} facets of anatase TiO_2 by adding HF during the preparation process. At the optimal facet ratio of {101} to {001} with 45 to 55 (adding 4.5 mL HF), TiO_2 exhibited the maximum CH_4 formation rate (1.35 μmol g^{-1} h^{-1}). The schematic of {001}

Table 6 Comparison of the typical phase or facet TiO_2 heterojunction systems

Photocatalyst	Solvent	Light source	Time[a]	Formation rate[b]	QE[c] (%)	Reference
Phase heterojunction						
TiO_2–RMA	H_2O	Hg lamp	8	CH_4: 2.36	—	228
Mixed-phase TiO_2	Sodium bicarbonate + H_2O + isopropanol	Hg lamp	3	CH_4: 34.67	—	229
Mixed-phase TiO_2	H_2O	Hg lamp	4	CH_4: 26.79	—	225
AuPd/3DOM-TiO_2	H_2O	Xe lamp	6	CH_4: 18.5	0.41	231
Anatase–brookite TiO_2	H_2O	Xe lamp	9	CH_3OH: 0.478	0.0717	232
Anatase–brookite TiO_2	H_2O	Solar simulator	4	CO: 2.1	—	234
Facet heterojunction						
{101}/{001} TiO_2	H_2O	Xe lamp	—	CH_4: 1.35	—	235
N-TiO_2-{101}/{001}	H_2O	Xe lamp	2	CH_3OH: 0.36	—	236
G/TiO_2-001/101	H_2O	Xe lamp	4	CO: 70.8 CH_4: 27.4	CO: 0.0557 CH_4: 0.0864	237
Pt/TiO_2-{001/101}@rGO	H_2O	Xe lamp	8	CH_4: 41.3	1.93	238
TiO_2-{110}/{111}	0.08 M $NaHCO_3$	Xe lamp	5	CH_3OH: 0.569	0.00569	239

[a] Irradiation time, h. [b] Formation rate, μmol g^{-1} h^{-1}. [c] Quantum efficiency (%).

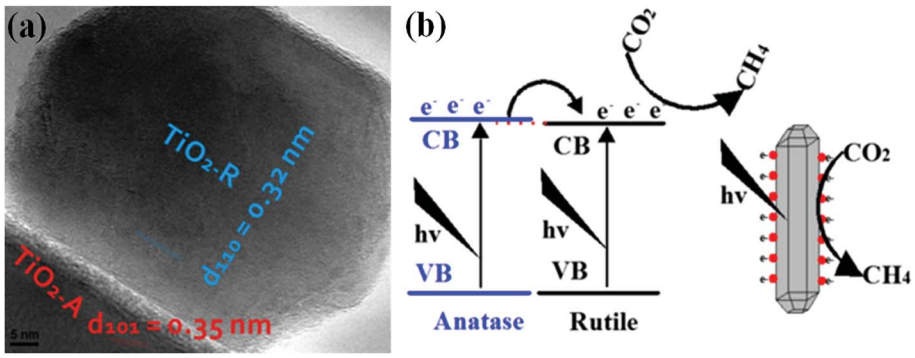

Fig. 22 (a) HRTEM image of TiO_2–RMA; (b) possible mechanism of TiO_2–RMA. Reproduced from ref. 228 with permission from Elsevier.

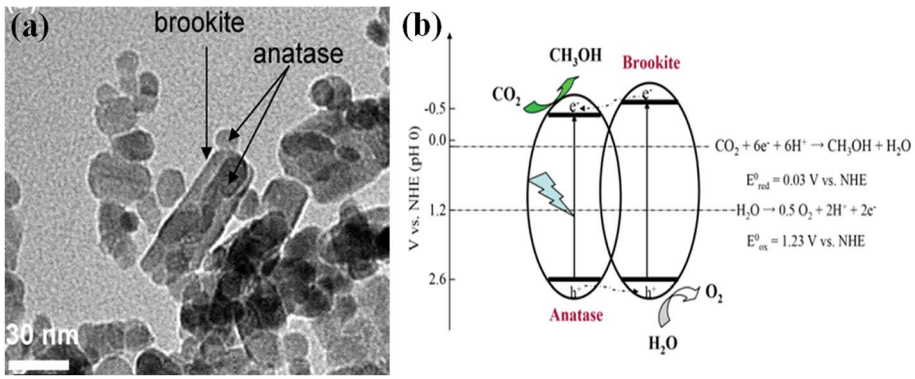

Fig. 23 (a) TEM image of anatase–brookite TiO_2; (b) possible mechanism of anatase–brookite TiO_2. Reproduced from ref. 232 with permission from Elsevier.

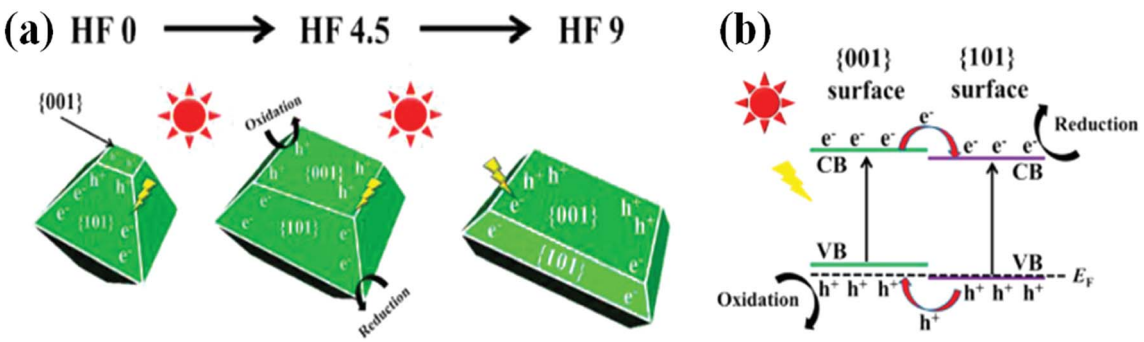

Fig. 24 (a) Schematic with tuning {001} and {101} facets of anatase TiO_2 by HF0, HF4.5, and HF9 samples; (b) charge transfer of {001} and {101} facets heterojunction of TiO_2. Reproduced from ref. 235 with permission from the American Chemical Society.

and {101} facet heterojunction is shown in Fig. 24b. Under light irradiation, e^- and h^+ could effectively transfer to the {101} and {001} facets, respectively. Therefore, {101} and {001} facets served as the reduction and oxidation activity sites, respectively. The {101} and {001} facets could form a facet heterojunction to enhance the photocatalytic performance. In another study, N-doped TiO_2 with 65% {001} and 35% {101} exposed facets obtained *via* a facile hydrothermal method was synthesized by Yu *et al.*[236] The improved CH_3OH formation rate was ascribed to the synergistic effect between the facet heterojunction, N doping, and surface fluorination.

Due to the unique properties of GR, it is often used as a cocatalyst to enhance the photocatalytic activity. GR loaded on coexposed {001} and {101} facets of TiO_2 (GR/TiO_2-001/101) was reported by Zhao *et al.*[237] The {001} and {101} facets could form the facet heterojunction, which, along with GR, could accelerate the separation of e^- and h^+ to increase the CO yield. In a subsequent work, Zhao *et al.* synthesized Pt/TiO_2@rGO core–shell-structured photocatalysts, where TiO_2 had 51% {001} and 49% {101} coexposed facets.[238] Pt NPs could gather and transfer e^- from TiO_2 and then transfer to rGO, resulting in high charge separation efficiency. The addition of cocatalysts of Pt NPs and

rGO could lead to a high CH_4 formation rate and quantum efficiency. Recently, Truong *et al.* found that the exposed high-index {311} facets of rutile TiO_2 nanocrystals comprised two {110} terraces and one {111} step.[239] Each branched nanocrystal was bound with four facets of the high-index {331} facet. It was interesting to note that the flower-like particles had a higher CH_3OH yield (0.569 μmol g^{-1} h^{-1}) than that of rod-like particles (0.388 μmol g^{-1} h^{-1}) for the photocatalytic reduction of CO_2.

4.5 Other TiO_2-based heterojunctions

Dye molecules are usually chemisorbed on the surface of TiO_2 for sensitization. Kang *et al.* reported the TDQD [(*E*)-3-(5-(4-(5-(4-(bis(4-(hexyloxy)phenyl)amino)phenyl)thiophen-2-yl)-6,7-diethyl-[1,2,5]thiadiazolo[3,4-*g*]quinoxalin-9-yl)thiophen-2-y)-2-cyanoacrylic acid] dye loaded onto commercialized TiO_2 (P25) to extend the visible light absorption region.[240] It exhibited a high CH_4 yield of about 1290 μmol g^{-1} L^{-1} after 8 h of light irradiation. Metal–organic frameworks (MOFs) are promising materials for CO_2 reduction due to their high surface area to enhance CO_2 adsorption. Petit *et al.* fabricated NH_2-UiO-66/TiO_2 nanosheet heterojunctions *via* an *in situ* growth method for the first time.[241] The heterostructure could offer a high surface area and more active sites. Moreover, the large CO_2 adsorption capacity could improve the CO_2 level on the surface of TiO_2 to react with the active sites to produce CO. Recently, hierarchical P25@microporous Co–Al-layered double hydroxides (Co–Al-LDHs) heterojunction for the photocatalytic reduction of CO_2 with high activity and selectivity to produce CO was also described.[242] Here, e^- could transfer from the Co–Al-LDH to P25; in contrast, h^+ could transfer from P25 to Co–Al-LDH. Therefore, e^- and h^+ were effectively separated. This may offer a facile method to design and fabricate LDH-based materials for energy conversion and pollutant degradation.

5. Conclusions and perspectives

In summary, this review discusses the design and fabrication of TiO_2-based heterojunction photocatalysts for the photocatalytic reduction of CO_2 into solar fuels. The photocatalytic reduction of CO_2 into solar fuels is a promising method to overcome energy crises and environmental problems. However, the photocatalytic reduction of CO_2 is far away from industrial applications.[102,243–245] On one hand, there are some common bottlenecks in this process. The energy efficiency that evaluates the transformation of photon energy into chemical energy is very low. For example, Chen *et al.* reported the energy efficiency was 1.158% by NiO/$InTaO_4$ under visible light illumination.[246] Furthermore, the instantaneous oxidation of the formed hydrocarbons may occur during CO_2 reduction; therefore, we should minimize hydrocarbon conversion under process conditions needed for CO_2 reduction.[247] In addition, hydrocarbons might be retained on the surface of the catalysts during the synthesis processes; therefore, we should eliminate the impact as much as possible. On the other hand, the selectivity of the desired products is low because the HER reaction is accompanied by CO_2 reduction, and it is a rather complex process.[248] CO, CH_4, HCOOH, CH_3OH, HCHO, C_2H_4, and CH_3-CH_2OH can be observed in some catalytic systems. The adsorption and activation of CO_2 onto the surface of catalysts can play some important roles in improving the selectivity toward the desired products. The increase in the catalyst surface area, introduction of surface defects (*e.g.*, oxygen and sulfur vacancies), and noble-metal cocatalysts have been widely selected strategies to enhance the adsorption and activation of CO_2.[249] The mechanism of CO_2 reduction should be comprehensively investigated in future studies. At the molecular level through *in situ* characterization techniques, we can better understand the reaction pathways of CO_2 reduction. The reaction barriers and rate-determining steps of CO_2 reduction have an important effect to enhance the conversion efficiency.

Developing efficient photocatalysts is the key for improving the photocatalytic reduction of CO_2. The attractive properties of heterojunction photocatalysts can be used to increase the charge separation and suppress the recombination of e^-/h^+ pairs. Therefore, designing a heterojunction is an effective strategy for high-activity photocatalysts in the photocatalytic reduction of CO_2. Currently, TiO_2-based heterojunction photocatalysts for the photocatalytic reduction of CO_2 are still in their early stages of development, and we believe that there is room for developing novel, powerful photocatalysts for CO_2 reduction. Interfacial or heterojunction quantitative control, facet control, surface decorations, band structure alignment, and interfacial *in situ* characterization on the heterojunction photocatalysts can also be critically important toward efficient photocatalysis, which should be further investigated.

At the same time, other strategies for the photocatalytic reduction of CO_2 are of equal importance. First, the adsorption of CO_2 over the surface of the photocatalyst is a very important step for the photocatalytic reduction of CO_2. The basic metal oxide can increase the adsorption of CO_2 and it can serve as a cocatalyst for contributing toward the photocatalytic reduction of CO_2. Second, the morphology has an important effect on the photocatalytic performance. It influences the surface structure, which can control the energy band position and surface reactivity, and affects the transfer of photogenerated carriers. Third, the size of the photocatalyst particles also influences the photocatalytic activity. The optimum particle size of the photocatalyst affects the charge-carrier dynamics and light-harvesting efficiency. A decrease in the particle size may increase the bandgap energy and decrease the light-harvesting efficiency. Fourth, the reductive half-reaction of CO_2 is coupled with the oxidative half-reaction of water oxidation to O_2. Further, more attention should be paid to the other half-reaction of water oxidation in future studies. In order to enhance the activity of CO_2 reduction, it can accelerate the oxidation reaction by adopting certain typical strategies for enhanced O_2 evolution in solar water splitting, such as adding some oxidizing auxiliaries.

Moreover, we also can develop other new types of photoreactors for the reduction of CO_2 to enhance the photocatalytic activity. Therefore, all the factors should be taken into account in the process of design and fabrication of the photocatalytic reduction of CO_2 into solar fuels. We hope that this review can

stimulate new insights and provide guidelines for future research at the intersection of the photocatalytic reduction of CO_2 into solar fuels, which can benefit humankind.

Conflicts of interest

There are no conflicts to declare.

Acknowledgements

This work was supported by the National Basic Research Program of China (2013CB933102), the National Natural Science Foundation of China (21567008, 21433008, 91545203 and 21503176), Program of 5511 Talents in Scientific and Technological Innovation of Jiangxi Province (20165BCB18014), Academic and Technical Leaders of the Main Disciplines in Jiangxi Province (20172BCB22018), Program of Qingjiang Excellent Young Talents, Jiangxi University of Science and Technology.

References

1 J. Peng, L. Lu and H. Yang, *Renewable Sustainable Energy Rev.*, 2013, **19**, 255–274.
2 B. Khezri, A. C. Fisher and M. Pumera, *J. Mater. Chem. A*, 2017, **5**, 8230–8246.
3 J. Zhao, X. Wang, Z. Xu and J. S. C. Loo, *J. Mater. Chem. A*, 2014, **2**, 15228–15233.
4 A. Álvarez, A. Bansode, A. Urakawa, A. V. Bavykina, T. A. Wezendonk, M. Makkee, J. Gascon and F. Kapteijn, *Chem. Rev.*, 2017, **117**, 9804–9838.
5 O. Ola and M. M. Maroto-Valer, *J. Photochem. Photobiol., C*, 2015, **24**, 16–42.
6 R. Shi, G. I. N. Waterhouse and T. Zhang, *Sol. RRL*, 2017, **1**, 1700126.
7 N. Pegiosa, V. Bliznukb, S. Prüntec, J. M. Schneiderc, R. Palkovits and K. Simeonov, *RSC Adv.*, 2018, **8**, 606–618.
8 G. Gao, Y. Jiao, E. R. Waclawik and A. Du, *J. Am. Chem. Soc.*, 2016, **138**, 6292–6297.
9 G. Yin, M. Nishikawa, Y. Nosaka, N. Srinivasan, D. Atarashi, E. Sakai and M. Miyauchi, *ACS Nano*, 2015, **9**, 2111–2119.
10 W. Wang, W. An, B. Ramalingam, S. Mukherjee, D. M. Niedzwiedzki, S. Gangopadhyay and P. Biswas, *J. Am. Chem. Soc.*, 2012, **134**, 11276–11281.
11 Y. Zhu, Z. Xu, W. Jiang, S. Zhong, L. Zhao and S. Bai, *J. Mater. Chem. A*, 2017, **5**, 2619–2628.
12 K. H. Kim, S. Kim, B. C. Moon, J. W. Choi, H. M. Jeong, Y. Kwon, S. Kwon, H. S. Choib and J. K. Kang, *J. Mater. Chem. A*, 2017, **5**, 8274–8279.
13 G. R. Dey, A. D. Belapurkar and K. Kishore, *J. Photochem. Photobiol., A*, 2004, **163**, 503–508.
14 R. Kuriki, H. Matsunaga, T. Nakashima, K. Wada, A. Yamakata, O. Ishitani and K. Maeda, *J. Am. Chem. Soc.*, 2016, **138**, 5159–5170.
15 S. Kaneco, Y. Ueno, H. Katsumata, T. Suzuki and K. Ohta, *Chem. Eng. J.*, 2006, **119**, 107–112.
16 L. Roy, P. M. Zimmerman and A. Paul, *Chem.–Eur. J.*, 2011, **17**, 435–439.
17 Q. Shen, X. Huang, J. Liu, C. Guo and G. Zhao, *Appl. Catal., B*, 2017, **201**, 70–76.
18 H. Zhou, T. Fan and D. Zhang, *ChemCatChem*, 2011, **3**, 513–528.
19 X. Huang, Q. Shen, J. Liu, N. Yang and G. Zhao, *Energy Environ. Sci.*, 2016, **9**, 3161–3171.
20 S. Wang, B. Guan and X. W. D. Lou, *Energy Environ. Sci.*, 2018, **11**, 306–310.
21 T. Inoue, A. Fujishima, S. Konishi and K. Honda, *Nature*, 1979, **277**, 637–638.
22 I. Hashemizadeh, V. B. Golovko, J. Choi, D. C. W. Tsang and A. C. K. Yip, *Chem. Eng. J.*, 2018, **347**, 64–73.
23 C. Dong, C. Lian, S. Hu, Z. Deng, J. Gong, M. Li, H. Liu, M. Xing and J. Zhang, *Nat. Commun.*, 2018, **9**, 1252.
24 B. Yu, Y. Zhou, P. Li, W. Tu, P. Li, L. Tang, J. Ye and Z. Zou, *Nanoscale*, 2016, **8**, 11870–11874.
25 Y. Ma, X. Wang, Y. Jia, X. Chen, H. Han and C. Li, *Chem. Rev.*, 2014, **114**, 9987–10043.
26 A. Nikokavoura and C. Trapalis, *Appl. Surf. Sci.*, 2017, **391**, 149–174.
27 H. Li, Y. Gao, Z. Xiong, C. Liao and K. Shih, *Appl. Surf. Sci.*, 2018, **439**, 552–559.
28 D. Xu, B. Cheng, W. Wang, C. Jiang and J. Yu, *Appl. Catal., B*, 2018, **231**, 368–380.
29 L. Lin, C. Hou, X. Zhang, Y. Wang, Y. Chen and T. He, *Appl. Catal., B*, 2018, **221**, 312–319.
30 Z. Jiang, W. Wan, H. Li, S. Yuan, H. Zhao and P. Wong, *Adv. Mater.*, 2018, **30**, 1706108.
31 A. Kumar, A. Kumar, G. Sharma, A. H. Al-Muhtaseb, M. Naushad, A. A. Ghfar, C. S. Guo and F. J. Stadler, *Chem. Eng. J.*, 2018, **339**, 393–410.
32 X. Jiao, Z. Chen, X. Li, Y. Sun, S. Gao, W. Yan, C. Wang, Q. Zhang, Y. Lin, Y. Luo and Y. Xie, *J. Am. Chem. Soc.*, 2017, **139**, 7586–7594.
33 S. Wang, B. Guan and X. W. D. Lou, *J. Am. Chem. Soc.*, 2018, **140**, 5037–5040.
34 J. Chen, F. Xin, X. Yin, T. Xiang and Y. Wang, *RSC Adv.*, 2015, **5**, 3833–3839.
35 G. Yang, D. Chen, H. Ding, J. Feng, J. Zhang, Y. Zhu, S. Hamid and D. W. Bahnemann, *Appl. Catal., B*, 2017, **219**, 611–618.
36 L. Xiao, R. Lin, J. Wang, C. Cui, J. Wang and Z. Li, *J. Colloid Interface Sci.*, 2018, **523**, 151–158.
37 S. Cao, B. Shen, T. Tong, J. Fu and J. Yu, *Adv. Funct. Mater.*, 2018, 1800136.
38 Z. Jiang, X. Liang, H. Zheng, Y. Liu, Z. Wang, P. Wang, X. Zhang, X. Qin, Y. Dai, M. H. Whangbo and B. Huang, *Appl. Catal., B*, 2017, **219**, 209–215.
39 M. Wang, Q. Han, L. Li, L. Tang, H. Li, Y. Zhou and Z. Zou, *Nanotechnology*, 2017, **28**, 1–8.
40 H. Cheng, B. Huang, Y. Liu, Z. Wang, X. Qin, X. Zhang and Y. Dai, *Chem. Commun.*, 2012, **48**, 9729–9731.
41 X. Kong, Y. Y. Choo, S. Chai, A. K. Soh and A. R. Mohamed, *Chem. Commun.*, 2016, **52**, 14242–14245.

42 P. Wang, Y. Bai, P. Luo and J. Liu, *Catal. Commun.*, 2013, **38**, 82–85.
43 Q. Li, B. Guo, J. Yu, J. Ran, B. Zhang, H. Yan and J. Gong, *J. Am. Chem. Soc.*, 2011, **133**, 10878–10884.
44 X. Pan and Y. Xu, *J. Phys. Chem. C*, 2015, **119**, 7184–7194.
45 W. Tu, Y. Zhou, Q. Liu, S. Yan, S. Bao, X. Wang, M. Xiao and Z. Zou, *Adv. Funct. Mater.*, 2013, **23**, 1743–1749.
46 Y. Liang, B. K. Vijayan, K. A. Gray and M. C. Hersam, *Nano Lett.*, 2011, **11**, 2865–2870.
47 S. Ijaz, M. F. Ehsan, M. N. Ashiq, N. Karamat and T. He, *Appl. Surf. Sci.*, 2016, **390**, 550–559.
48 Y. Wei, J. Jiao, Z. Zhen, J. Liu, J. Li, G. Jiang, Y. Wang and A. Duan, *Appl. Catal., B*, 2015, **179**, 422–432.
49 S. Wang and X. Wang, *Appl. Catal., B*, 2015, **162**, 494–500.
50 P. Praus, O. Kozák, K. Kočí, A. Panáček and R. Dvorský, *J. Colloid Interface Sci.*, 2011, **360**, 574–579.
51 S. Xie, Y. Wang, Q. Zhang, W. Deng and Y. Wang, *Chem. Commun.*, 2015, **51**, 3430–3433.
52 Y. He, Y. Wang, L. Zhang, B. Teng and M. Fan, *Appl. Catal., B*, 2015, **168–169**, 1–8.
53 Q. Guo, Q. Zhang, H. Wang and Z. Zhao, *Catal. Commun.*, 2018, **103**, 24–28.
54 S. R. Lingampalli, M. M. Ayyub, G. Magesh and C. N. R. Rao, *Chem. Phys. Lett.*, 2018, **691**, 28–32.
55 K. Li, B. Peng and T. Peng, *ACS Catal.*, 2016, **6**, 7485–7527.
56 W. Yuan, L. Cheng, Y. An, S. Lv, H. Wu, X. Fan, Y. Zhang, X. Guo and J. Tang, *Adv. Sci.*, 2018, 1700870.
57 M. Ge, C. Cao, J. Huang, S. Li, Z. Chen, K. Zhang, S. S. Al-Deyabd and Y. Lai, *J. Mater. Chem. A*, 2016, **4**, 6772–6801.
58 J. Pan, X. Wu, L. Wang, G. Liu, G. Q. M. Lu and H. Cheng, *Chem. Commun.*, 2011, **47**, 8361–8363.
59 J. F. d. Brito and M. V. B. Zanoni, *Chem. Eng. J.*, 2017, **318**, 264–271.
60 J. Low, B. Cheng and J. Yu, *Appl. Surf. Sci.*, 2017, **392**, 658–686.
61 S. Xie, Y. Wang, Q. Zhang, W. Deng and Y. Wang, *ACS Catal.*, 2014, **4**, 3644–3653.
62 S. Xie, Y. Wang, Q. Zhang, W. Fan, W. Deng and Y. Wang, *Chem. Commun.*, 2013, **49**, 2451–2453.
63 G. Liu, S. Xie, Q. Zhang, Z. Tian and Y. Wang, *Chem. Commun.*, 2015, **51**, 13654–13657.
64 Q. Zhai, S. Xie, W. Fan, Q. Zhang, Y. Wang, W. Deng and Y. Wang, *Angew. Chem., Int. Ed.*, 2013, **52**, 5776–5779.
65 C. Yu, L. Wei, J. Chen, Y. Xie, W. Zhou and Q. Fan, *Ind. Eng. Chem. Res.*, 2014, **53**, 5759–5766.
66 C. Yu, L. Wei, W. Zhou, J. Chen, Q. Fan and H. Liu, *Appl. Surf. Sci.*, 2014, **319**, 312–318.
67 C. Yu, L. Wei, J. Chen, W. Zhou, Q. Fan and J. Yu, *Rare Met.*, 2016, **35**, 475–480.
68 C. Yu, J. Chen, W. Zhou, L. Wei and Q. Fan, *Mater. Res. Innovations*, 2015, **19**, 54–58.
69 J. Tian, Z. Zhao, A. Kumar, R. I. Boughton and H. Liu, *Chem. Soc. Rev.*, 2014, **43**, 6920–6937.
70 J. Tian, Z. Wu, Z. Liu, C. Yu, K. Yang, L. Zhu, W. Huang and Y. Zhou, *Chin. J. Catal.*, 2017, **38**, 1899–1908.
71 C. Yu, G. Li, S. Kumar, K. Yang and R. Jin, *Adv. Mater.*, 2014, **26**, 892–898.
72 J. Jin, J. Yu, D. Guo, C. Cui and W. Ho, *Small*, 2015, **11**, 5262–5271.
73 H. Li, X. Zhang and D. R. MacFarlane, *Adv. Energy Mater.*, 2015, **5**, 1401077.
74 X. Jiao, X. Li, X. Jin, Y. Sun, J. Xu, L. Liang, H. Ju, J. Zhu, Y. Pan, W. Yan, Y. Lin and Y. Xie, *J. Am. Chem. Soc.*, 2017, **49**, 18044–18051.
75 Z. Wang, K. Teramura, Z. Huang, S. Hosokawa, Y. Sakata and T. Tanaka, *Catal. Sci. Technol.*, 2016, **6**, 1025–1032.
76 H. Shi, G. Chen, C. Zhang and Z. Zou, *ACS Catal.*, 2014, **4**, 3637–3643.
77 Y. He, L. Zhang, M. Fan, X. Wang, M. L. Walbridge, Q. Nong, Y. Wu and L. Zhao, *Sol. Energy Mater. Sol. Cells*, 2015, **137**, 175–184.
78 T. W. Kim, I. Y. Kim, T. S. Jung, C. H. Ko and S. J. Hwang, *Adv. Funct. Mater.*, 2013, **23**, 4377–4385.
79 G. Bucher and W. Sander, *Science*, 2014, **346**, 544–545.
80 S. Nasri, Y. Ajili, N. E. Jaidane, Y. N. Kalugina, P. Halvick, T. Stoecklin and M. Hochlaf, *J. Chem. Phys.*, 2015, **142**, 174301–174308.
81 J. R. Bolton, *Science*, 1978, **202**, 705–711.
82 J. M. Lehn and R. Ziessel, *Proc. Natl. Acad. Sci. U. S. A.*, 1982, **79**, 701–704.
83 I. Willner, R. Maidan, D. Mandler, H. Dum, G. Dorr and K. Zengerlet, *J. Am. Chem. Soc.*, 1987, **109**, 6080–6086.
84 L. Guo, Y. Wang and T. He, *Chem. Rec.*, 2016, **16**, 1918–1933.
85 V. P. Indrakanti, J. D. Kubickib and H. H. Schobert, *Energy Environ. Sci.*, 2009, **2**, 745–758.
86 B. Kumar, M. Llorente, J. Froehlich, T. Dang, A. Sathrum and C. P. Kubiak, *Annu. Rev. Phys. Chem.*, 2012, **63**, 541–569.
87 A. J. Morris, G. J. Meyer and E. Fujita, *Acc. Chem. Res.*, 2009, **42**, 1983–1994.
88 E. E. Benson, C. P. Kubiak, A. J. Sathrum and J. M. Smieja, *Chem. Soc. Rev.*, 2009, **38**, 89–99.
89 A. H. Yahaya, M. A. Gondal and A. Hameed, *Chem. Phys. Lett.*, 2004, **400**, 206–212.
90 A. D. Handoko, K. Li and J. W. Tang, *Curr. Opin. Chem. Eng.*, 2012, **2**, 200–206.
91 K. Maeda and K. Domen, *J. Phys. Chem. C*, 2007, **111**, 7851–7861.
92 O. Carp, C. L. Huisman and A. Reller, *Prog. Solid State Chem.*, 2004, **32**, 33–177.
93 U. G. Akpan and B. H. Hameed, *J. Hazard. Mater.*, 2009, **170**, 520–529.
94 K. Koci, L. Obalova and Z. Lacny, *Chem. Pap.*, 2008, **62**, 1–9.
95 A. Dhakshinamoorthy, S. Navalon, A. Corma and H. Garcia, *Energy Environ. Sci.*, 2012, **5**, 9217–9233.
96 J. Chen, F. Xin, S. Qin and X. Yin, *Chem. Eng. J.*, 2013, **230**, 506–512.
97 G. Zeng, J. Qiu, Z. Li, P. Pavaskar and S. B. Cronin, *ACS Catal.*, 2014, **4**, 3512–3516.
98 M. Gui, S. Chai and A. R. Mohamed, *Appl. Surf. Sci.*, 2014, **319**, 37–43.
99 L. Yuan and Y. Xu, *Appl. Surf. Sci.*, 2015, **342**, 154–167.
100 S. Rani, N. Bao and S. C. Roy, *Appl. Surf. Sci.*, 2014, **289**, 203–208.

101 S. Xie, Q. Zhang, G. Liu and Y. Wang, *Chem. Commun.*, 2016, **52**, 35–59.
102 S. N. Habisreutinger, L. Schmidt-Mende and J. K. Stolarczyk, *Angew. Chem., Int. Ed.*, 2013, **52**, 7372–7408.
103 X. Li, J. Wen, J. Low, Y. Fang and J. Yu, *Sci. China Mater.*, 2014, **57**, 70–100.
104 J. L. White, M. F. Baruch, J. E. Pander, Y. Hu, I. C. Fortmeyer, J. E. Park, T. Zhang, K. Liao, J. Gu, Y. Yan, T. W. Shaw, E. Abelev and A. B. Bocarsly, *Chem. Rev.*, 2015, **115**, 12888–12935.
105 A. L. Linsebigler, G. Lu and J. T. Yates, *Chem. Rev.*, 1995, **95**, 735–758.
106 H. Jiao, X. Yu, Z. Liu, P. Kuang and Y. Zhang, *RSC Adv.*, 2015, **5**, 16239–16249.
107 R. Chen, S. Pang, H. An, J. Zhu, S. Ye, Y. Gao, F. Fan and C. Li, *Nat. Energy*, 2018, **3**, 655–663.
108 Z. T. Hu, J. Liu, X. Yan, W. D. Oh and T. T. Lim, *Chem. Eng. J.*, 2015, **262**, 1022–1032.
109 Z. Y. Asu, M. Yoshiteru, M. Yasuaki and H. I. Nilsun, *Appl. Catal., B*, 2015, **172–173**, 7–17.
110 G. Liu, L. Wang, H. Yang, H. Cheng and G. Lu, *J. Mater. Chem.*, 2010, **20**, 831–843.
111 L. Zhang, Y. Li, Q. Zhang and H. Wang, *CrystEngComm*, 2013, **15**, 5986–5993.
112 L. Wang, J. Ge, A. Wang, M. Deng, X. Wang, S. Bai, R. Li, J. Jiang, Q. Zhang, Y. Luo and Y. Xiong, *Angew. Chem.*, 2014, **53**, 5107–5111.
113 Y. Jia, S. Shen, D. Wang, X. Wang, J. Shi, F. Zhang, H. Han and C. Li, *J. Mater. Chem. A*, 2013, **1**, 7905–7912.
114 Z. Gan, X. Wu, M. Meng, X. Zhu, L. Yang and P. Chu, *ACS Nano*, 2014, **8**, 9304–9310.
115 Y. Gu, M. Xing and J. Zhang, *Appl. Surf. Sci.*, 2014, **319**, 8–15.
116 M. Bideau, B. Claudel, C. Dubien, L. Faure and H. Kazouan, *J. Photochem. Photobiol., A*, 1995, **91**, 137–144.
117 S. N. Habisreutinger, L. Schmidt-Mende and J. K. Stolarczyk, *Angew. Chem., Int. Ed.*, 2013, **52**, 7372–7408.
118 A. Corma and H. Garcia, *J. Catal.*, 2013, **308**, 168–175.
119 Z. Xiong, Z. Lei, B. Gong, X. Chen, Y. Zhao, J. Zhang, C. Zheng and J. C. S. Wu, *Catal. Commun.*, 2017, **89**, 4–8.
120 V. H. Nguyen and J. C. S. Wu, *Appl. Catal., A*, 2018, **550**, 122–141.
121 H. Wu, N. H. Nguyen, H. Bai, S. Chang and J. C. S. Wu, *RSC Adv.*, 2015, **5**, 63142–63151.
122 O. Ola, M. Maroto-Valer, D. Liu, S. Mackintosh, C. W. Lee and J. C. S. Wu, *Appl. Catal., B*, 2012, **126**, 172–179.
123 W. H. Lee, C. H. Liao, M. F. Tsai, C. W. Huang and J. C. S. Wu, *Appl. Catal., B*, 2013, **132–133**, 445–451.
124 Z. Y. Wang, H. C. Chou, J. C. S. Wu, D. P. Tsai and G. Mul, *Appl. Catal., A*, 2010, **380**, 172–177.
125 J. C. S. Wu, H. M. Lin and C. L. Lai, *Appl. Catal., A*, 2005, **296**, 194–200.
126 J. C. S. Wu, T. H. Wu, T. Chu, H. Huang and D. Tsai, *Top. Catal.*, 2008, **47**, 131–136.
127 T. V. Nguyen and J. C. S. Wu, *Appl. Catal., A*, 2008, **335**, 112–120.
128 K. Yuan, L. Yang, X. Du and Y. Yang, *Energy Convers. Manage.*, 2014, **81**, 98–105.
129 P. Usubharatana, D. McMartin, A. Veawab and P. Tontiwachwuthikul, *Ind. Eng. Chem. Res.*, 2006, **45**, 2558–2568.
130 P. Y. Liou, S. C. Chen, J. C. S. Wu, D. Liu, S. Mackintosh, M. Maroto-Valer and R. Linforth, *Energy Environ. Sci.*, 2011, **4**, 1487–1494.
131 M. Tahir and N. S. Amin, *Chem. Eng. J.*, 2013, **230**, 314–327.
132 M. Tahir and B. Tahir, *Appl. Surf. Sci.*, 2016, **377**, 244–252.
133 X. Cheng, R. Chen, X. Zhu, Q. Liao, L. An, D. Ye, X. He, S. Li and L. Li, *Energy*, 2017, **120**, 276–282.
134 M. Cheng, S. Yang, R. Chen, X. Zhu, Q. Liao and Y. Huang, *Int. J. Hydrogen Energy*, 2017, **42**, 9722–9732.
135 X. Cheng, R. Chen, X. Zhu, Q. Liao, X. He, S. Li and L. Li, *Int. J. Hydrogen Energy*, 2016, **41**, 2457–2465.
136 H. Wang, L. Zhang, Z. Chen, J. Hu, S. Li, Z. Wang, J. Liu and X. Wang, *Chem. Soc. Rev.*, 2014, **43**, 5234–5244.
137 P. Zhou, J. Yu and M. Jaroniec, *Adv. Mater.*, 2014, **26**, 4920–4935.
138 S. Bai, J. Jiang, Q. Zhang and Y. Xiong, *Chem. Soc. Rev.*, 2015, **44**, 2893–2939.
139 K. Maeda, *ACS Catal.*, 2013, **3**, 1486–1503.
140 D. Zeng, K. Yang, C. Yu, F. Chen, X. Li, Z. Wu and H. Liu, *Appl. Catal., B*, 2018, **237**, 449–463.
141 C. C. Yang, Y. H. Yu, B. van der Linden, J. C. S. Wu and G. Mul, *J. Am. Chem. Soc.*, 2010, **132**, 8398–8406.
142 L. Yu, G. Li, X. Zhang, X. Ba, G. Shi, Y. Li, P. K. Wong, J. Yu and Y. Yu, *ACS Catal.*, 2016, **6**, 6444–6454.
143 X. An, K. Li and J. Tang, *ChemSusChem*, 2014, **7**, 1086–1093.
144 M. L. Ovcharov, A. M. Mishura, N. D. Shcherban, S. M. Filonenko and V. M. Granchak, *Sol. Energy*, 2016, **139**, 452–457.
145 H. Xu, S. Ouyang, L. Liu, D. Wang, T. Kako and J. Ye, *Nanotechnology*, 2014, **25**, 165402.
146 F. Bi, M. F. Ehsan, W. Liu and T. He, *Chin. J. Chem.*, 2015, **33**, 112–118.
147 D. Liu, Y. Fernández, O. Ola, S. Mackintosh, M. Maroto-Valer, C. M. A. Parlett, A. F. Lee and J. C. S. Wu, *Catal. Commun.*, 2012, **25**, 78–82.
148 M. A. M. Júnior, A. Morais and A. F. Nogueira, *Microporous Mesoporous Mater.*, 2016, **234**, 1–11.
149 J. Wang, G. Ji, Y. Liu, M. A. Gondal and X. Chang, *Catal. Commun.*, 2014, **46**, 17–21.
150 Y. Li, W. Zhang, X. Shen, P. Peng, L. Xiong and Y. Yu, *Chin. J. Catal.*, 2015, **36**, 2229–2236.
151 H. R. Kim, A. Razzaq, C. A. Grimes and S. I. In, *J. CO_2 Util.*, 2017, **20**, 91–96.
152 Q. Zhang, L. Huang, S. Kang, C. Yin, Z. Ma, L. Cui and Y. Wang, *RSC Adv.*, 2017, **7**, 43642–43647.
153 R. Gusain, P. Kumar, O. P. Sharma, S. L. Jain and O. P. Khatri, *Appl. Catal., B*, 2016, **181**, 352–362.
154 M. H. Razali and M. Yusoff, *Mater. Lett.*, 2018, **221**, 168–171.
155 M. Akbari and S. Sharifnia, *Mater. Lett.*, 2017, **194**, 110–113.
156 A. Yarahmadi and S. Sharifnia, *Dyes Pigm.*, 2014, **107**, 140–145.
157 S. Qin, F. Xin, Y. Liu, X. Yin and W. Ma, *J. Colloid Interface Sci.*, 2011, **356**, 257–261.

158 S. Slamet, H. W. Nasution, E. Purnama, S. Kosela and J. Gunlazuardi, *Catal. Commun.*, 2005, **6**, 313–319.
159 B. Fang, Y. Xing, A. Bonakdarpour, S. Zhang and D. P. Wilkinson, *ACS Sustainable Chem. Eng.*, 2015, **3**, 2381–2388.
160 S. M. Park, A. Razzaq, Y. H. Park, S. Sorcar, Y. Park, C. A. Grimes and S. I. In, *ACS Omega*, 2016, **1**, 868–875.
161 S. I. In, D. D. Vaughn II and R. E. Schaak, *Angew. Chem.*, 2012, **124**, 3981–3984.
162 Z. Zhang and J. Li, *J. Mater. Sci.*, 2011, **46**, 3590–3596.
163 G. Marcì, E. I. García-López and L. Palmisano, *Catal. Commun.*, 2014, **53**, 38–41.
164 Y. Zou, X. Wang, Y. Ai, Y. Liu, Y. Ji, H. Wang, T. Hayat, A. Alsaedi, W. Hu and X. Wang, *J. Mater. Chem. A*, 2016, **4**, 14170–14179.
165 Y. Pan, Z. Liu, W. Wang, C. Peng, K. Shi and X. Ji, *J. Mater. Chem. A*, 2016, **4**, 2537–2549.
166 N. R. Singha, M. Karmakar, M. Mahapatra, H. Mondal, A. Dutta, M. Deb, M. Mitra, C. Roy and P. K. Chattopadhyay, *J. Mater. Chem. A*, 2018, **6**, 8078–8100.
167 L. Cui, J. Wu and H. Ju, *ACS Appl. Mater. Interfaces*, 2014, **6**, 16210–16216.
168 C. Cao, C. Hua, W. Shen, S. Wang, Y. Tian and X. Wang, *J. Alloys Compd.*, 2012, **523**, 139–145.
169 G. Song, F. Xin, J. Chen and X. Yin, *Appl. Catal., A*, 2014, **473**, 90–95.
170 S. Ding, X. Yin, X. Lü, Y. Wang, F. Huang and D. Wan, *ACS Appl. Mater. Interfaces*, 2012, **4**, 306–311.
171 A. A. Beigi, S. Fatemi and Z. Salehi, *J. CO_2 Util.*, 2014, **7**, 23–29.
172 X. Li, H. Liu, D. Luo, J. Li, Y. Huang, H. Li, Y. Fang, Y. Xu and L. Zhu, *Chem. Eng. J.*, 2012, **180**, 151–158.
173 C. Wang, R. L. Thompson, P. Ohodnicki, J. Baltrus and C. Matranga, *J. Mater. Chem.*, 2011, **21**, 13452–13457.
174 J. Jiao, Y. Wei, Z. Zhao, J. Liu, J. Li, A. Duan and G. Jiang, *Ind. Eng. Chem. Res.*, 2014, **53**, 17345–17354.
175 Y. Wang, B. Li, C. Zhang, L. Cui, S. Kang, X. Li and L. Zhou, *Appl. Catal., B*, 2013, **130–131**, 277–284.
176 W. Yu, D. Xu and T. Peng, *J. Mater. Chem. A*, 2015, **3**, 19936–19947.
177 G. Xi, S. Ouyang and J. Ye, *Chem.–Eur. J.*, 2011, **17**, 9057–9061.
178 Z. Xiong, Z. Lei, S. Ma, X. Chen, B. Gong, Y. Zhao, J. Zhang, C. Zheng and J. C. S. Wu, *Appl. Catal., B*, 2017, **219**, 412–424.
179 Q. D. Truong, J. Liu, C. Chung and Y. Ling, *Catal. Commun.*, 2012, **19**, 85–89.
180 Q. Kang, T. Wang, P. Li, L. Liu, K. Chang, M. Li and J. Ye, *Angew. Chem.*, 2015, **127**, 855–859.
181 M. Reli, P. W. Huo, M. Šihor, N. Ambrožová, I. Troppová, L. Matějová, J. Lang, L. Svoboda, P. Kuśtrowski, M. Ritz, P. Praus and K. Kočí, *J. Phys. Chem. A*, 2016, **120**, 8564–8573.
182 S. Zhou, Y. Liu, J. Li, Y. Wang, G. Jiang, Z. Zhao, D. Wang, A. Duan, J. Liu and Y. Wei, *Appl. Catal., B*, 2014, **158–159**, 20–29.
183 M. A. Asi, C. He, M. H. Su, D. Xia, L. Lin, H. Deng, Y. Xiong, R. Qiu and X. Li, *Catal. Today*, 2011, **175**, 256–263.
184 H. Li, S. Gan, H. Wang, D. Han and L. Niu, *Adv. Mater.*, 2015, **27**, 6906–6913.
185 T. Di, B. Zhu, B. Cheng, J. Yu and J. Xu, *J. Catal.*, 2017, **352**, 532–541.
186 Y. Liu, G. Ji, M. A. Dastageer, L. Zhu, J. Wang, B. Zhang, X. Chang and M. A. Gondal, *RSC Adv.*, 2014, **4**, 56961–56969.
187 G. Song, F. Xin and X. Yin, *J. Colloid Interface Sci.*, 2015, **442**, 60–66.
188 L. Kuai, Y. Zhou, W. Tu, P. Li, H. Li, Q. Xu, L. Tang, X. Wang, M. Xiao and Z. Zou, *RSC Adv.*, 2015, **5**, 88409–88413.
189 J. Q. Jiao, Y. C. Wei, Z. Zhao, W. J. Zhong, J. Liu, J. M. Li, A. J. Duan and G. Y. Jiang, *Catal. Today*, 2015, **258**, 319–326.
190 A. Ayati, A. Ahmadpour, F. F. Bamoharram, M. M. Heravi and M. Sillanpää, *Gold Bull.*, 2012, **45**, 145–151.
191 M. Gui, W. M. P. Wong, S. Chai and A. R. Mohamed, *Chem. Eng. J.*, 2015, **278**, 272–278.
192 C. Wang, K. M. Kwon, M. L. Odlyzko, B. H. Lee and M. Shim, *J. Phys. Chem. C*, 2007, **111**, 11734–11741.
193 C. Wang, R. L. Thompson, J. Baltrus and C. Matranga, *J. Phys. Chem. Lett.*, 2010, **1**, 48–53.
194 L. C. Sim, K. H. Leong, P. Saravanan and S. Ibrahim, *Appl. Surf. Sci.*, 2015, **358**, 122–129.
195 A. K. Geim and K. S. Novoselov, *Nat. Mater.*, 2007, **6**, 183–191.
196 W. Ong, L. Tan, S. Chai and S. Yong, *Chem. Commun.*, 2015, **51**, 858–861.
197 Y. Zhang, Z. Tang, X. Fu and Y. Xu, *ACS Nano*, 2010, **4**, 7303–7314.
198 W. Fan, Q. Zhang and Y. Wang, *Phys. Chem. Chem. Phys.*, 2013, **15**, 2632–2649.
199 A. A. Balandin, S. Ghosh, W. Bao, I. Calizo, D. Teweldebrhan, F. Miao and C. N. Lau, *Nano Lett.*, 2008, **8**, 902–907.
200 L. Tan, S. Chai and A. R. Mohamed, *ChemSusChem*, 2012, **5**, 1868–1882.
201 M. D. Stoller, S. J. Park, Y. Zhu, J. An and R. S. Ruoff, *Nano Lett.*, 2008, **8**, 3498–3502.
202 H. K. Chae, D. Y. Siberio-perez, J. Kim, Y. B. Go, M. Eddaoudi, A. J. Matzger, M. O'Keeffe and O. M. Yaghi, *Nature*, 2004, **427**, 523–527.
203 X. Li, J. Yu, S. Wageh, A. A. Al-Ghamdi and J. Xie, *Small*, 2016, **12**, 6640–6696.
204 L. S. Schadler, S. C. Giannarisg and P. M. Ajayan, *Appl. Phys. Lett.*, 1998, **73**, 3842–3844.
205 X. Du, I. Skachko, A. Barker and E. Y. Andrei, *Nat. Nanotechnol.*, 2008, **3**, 491–495.
206 K. I. Bolotin, K. J. Sikes, Z. Jiang, M. Klima, G. Fudenberg, J. Hone, P. Kim and H. L. Stormer, *Solid State Commun.*, 2008, **146**, 351–355.
207 R. R. Nair, P. Blake, A. N. Grigorenko, K. S. Novoselov, T. J. Booth, T. Stauber, N. M. R. Peres and A. K. Geim, *Science*, 2008, **320**, 1308.
208 K. S. Novoselov, A. K. Geim, S. V. Morozov, D. Jiang, Y. Zhang, S. V. Dubonos, I. V. Grigorieva and A. A. Firsov, *Science*, 2004, **306**, 666–669.

209 F. Li, L. Zhang, J. Tong, Y. Liu, S. Xu, Y. Cao and S. Cao, *Nano Energy*, 2016, **27**, 320–329.
210 W. Ong, L. Tan, S. Chai, S. Yong and A. R. Mohamed, *Nano Res.*, 2014, **7**, 1528–1547.
211 K. P. Loh, Q. Bao, G. Eda and M. Chhowalla, *Nat. Chem.*, 2010, **2**, 1015–1024.
212 Y. Zhang, N. Zhang, Z. Tang and Y. Xu, *J. Phys. Chem. C*, 2014, **118**, 5299–5308.
213 M. Yang, X. Pan, N. Zhang and Y. Xu, *CrystEngComm*, 2013, **15**, 6819–6828.
214 Y. Sun, Q. Wu and G. Shi, *Energy Environ. Sci.*, 2011, **4**, 1113–1132.
215 L. Han, P. Wang and S. Dong, *Nanoscale*, 2012, **4**, 5814–5825.
216 N. Zhang, Y. Zhang and Y. Xu, *Nanoscale*, 2012, **4**, 5792–5813.
217 G. Williams, B. Seger and P. V. Kamat, *ACS Nano*, 2008, **2**, 1487–1491.
218 L. Tan, W. Ong, S. Chai and A. R. Mohamed, *Nanoscale Res. Lett.*, 2013, **8**, 465.
219 L. Tan, W. Ong, S. Chai, B. T. Goh and A. R. Mohamed, *Appl. Catal., B*, 2015, **179**, 160–170.
220 L. Tan, W. Ong, S. Chai and A. R. Mohamed, *Appl. Catal., B*, 2015, **166–167**, 251–259.
221 Y. Zhang, D. Ma, Y. Zhang, W. Chen and S. Huang, *Nano Energy*, 2013, **2**, 545–552.
222 D. Mosconi, D. Mazzier, S. Silvestrini, A. Privitera, C. Marega, L. Franco and A. Moretto, *ACS Nano*, 2015, **9**, 4156–4164.
223 M. Li, M. Wang, L. Zhu, Y. Li, Z. Yan, Z. Shen and X. Cao, *Appl. Catal., B*, 2018, **231**, 269–276.
224 P. Li, S. Ouyang, G. Xi, T. Kako and J. Ye, *J. Phys. Chem. C*, 2012, **116**, 7621–7628.
225 P. Li, S. Ouyang, Y. Zhang, T. Kako and J. Ye, *J. Mater. Chem. A*, 2013, **1**, 1185–1191.
226 P. Li, H. Xu, L. Liu, T. Kako, N. Umezawa, H. Abe and J. Ye, *J. Mater. Chem. A*, 2014, **2**, 5606–5609.
227 D. Dambournet, I. Belharouak and K. Amine, *Chem. Mater.*, 2010, **22**, 1173–1179.
228 P. Wang, Y. Bai, J. Liu, Z. Fan and Y. Hu, *Catal. Commun.*, 2012, **29**, 185–188.
229 G. H. Li, S. Ciston, Z. V. Saponjic, L. Chen, N. M. Dimitrijevic, T. Rajh and K. A. Gray, *J. Catal.*, 2008, **253**, 105–110.
230 L. Chen, M. E. Graham, G. Li, D. R. Gentner, N. M. Dimitrijevic and K. A. Gray, *Thin Solid Films*, 2009, **517**, 5641–5645.
231 J. Jiao, Y. Wei, Y. Zhao, Z. Zhao, A. Duan, J. Liu, Y. Pang, J. Li, G. Jiang and Y. Wang, *Appl. Catal., B*, 2017, **209**, 228–239.
232 Q. D. Truong, T. Le, J. Liu, C. Chung and Y. Ling, *Appl. Catal., A*, 2012, **437–438**, 28–35.
233 K. Tomita, V. Petrykin, M. Kobayashi, M. Shiro, M. Yoshimura and M. Kakihana, *Angew. Chem., Int. Ed.*, 2006, **45**, 2378–2381.
234 H. Zhao, L. Liu, J. M. Andino and Y. Li, *J. Mater. Chem. A*, 2013, **1**, 8209–8216.
235 J. Yu, J. Low, W. Xiao, P. Zhou and M. Jaroniec, *J. Am. Chem. Soc.*, 2014, **136**, 8839–8842.
236 M. S. Akple, J. Low, Z. Qin, S. Wageh, A. A. Al-Ghamdi, J. Yu and S. Liu, *Chin. J. Catal.*, 2015, **36**, 2127–2134.
237 Z. Xiong, Y. Luo, Y. Zhao, J. Zhang, C. Zheng and J. C. S. Wu, *Phys. Chem. Chem. Phys.*, 2016, **18**, 13186–13195.
238 Y. Zhao, Y. Wei, X. Wu, H. Zheng, Z. Zhao, J. Liu and J. Li, *Appl. Catal., B*, 2018, **226**, 360–372.
239 Q. D. Truong, H. T. Hoa and T. S. Le, *J. Colloid Interface Sci.*, 2017, **504**, 223–229.
240 J. Y. Do, V. Tamilavan, R. Agneeswari, M. H. Hyun and M. Kang, *J. Photochem. Photobiol., A*, 2016, **330**, 30–36.
241 A. Crake, K. C. Christoforidis, A. Kafizas, S. Zafeiratos and C. Petit, *Appl. Catal., B*, 2017, **210**, 131–140.
242 S. Kumar, M. A. Isaacs, R. Trofimovaite, L. Durndell, C. M. A. Parlett, R. E. Douthwaite, B. Coulson, M. C. R. Cockett, K. Wilson and A. F. Lee, *Appl. Catal., B*, 2017, **209**, 394–404.
243 Y. Izumi, *Coord. Chem. Rev.*, 2013, **257**, 171–186.
244 K. Mori, H. Yamashita and M. Anpo, *RSC Adv.*, 2012, **2**, 3165–3172.
245 K. Li, X. An, K. H. Park, M. Khraisheh and J. Tang, *Catal. Today*, 2014, **224**, 3–12.
246 P. Pan and Y. Chen, *Catal. Commun.*, 2007, **8**, 1546–1549.
247 M. S. Hamdy, R. Amrollahi, I. Sinev, B. Mei and G. Mul, *J. Am. Chem. Soc.*, 2014, **136**, 594–597.
248 W. Tu, Y. Zhou and Z. Zou, *Adv. Mater.*, 2014, **26**, 4607–4626.
249 X. Chang, T. Wang and J. Gong, *Energy Environ. Sci.*, 2016, **9**, 2177–2196.